2

COMMISSARIAT A L'ENERGIE ATOMIQUE

CENTRE D'ETUDES NUCLEAIRES DE SACLAY
Service de Documentation
F91191 GIF SUR YVETTE CEDEX

CEA-CONF - - 7888

M 2

EVALUATION OF HIGH TEMPERATURE MECHANICAL PROPERTIES AND CONSTITUTIVE EQUATION OF AUSTENITIC STAINLESS STEELS

BLANCHARD, P.; TORTEL, J. -CEA,CEN Saclay, IRDI, DTech

Communication présentée à : International seminar on computer aided engineering for reactor structures
Brussels (Belgium) 26-27 Aug 1985

EVALUATION OF HIGH TEMPERATURE MECHANICAL PROPERTIES AND CONSTITUTIVE EQUATION OF AUSTENITIC STAINLESS STEELS

P. BLANCHARD, J. TORTEL

Commissariat à l'Energie Atomique - CEN SACLAY (IRDI/D Tech/SRMA)
91191 GIF-SUR-YVETTE CEDEX, FRANCE

COMMISSARIAT A L'ENERGIE ATOMIQUE
CEA TECHNOLOGIE
DIVISION DE METALLURGIE ET D'ETUDES DES COMBUSTIBLES NUCLEAIRES

26-27 Août 1985

POST SMIRT CONFERENCE

INELASTIC ANALYSIS AND LIFE PREDICTION

IN HIGH TEMPERATURE ENVIRONMENT

5th INTERNATIONAL SEMINAR SPONSORED

by ELECTRICITE DE FRANCE - S.E.P.T.E.N.

12-14, Avenue Dutriévoz - 69100 VILLEURBANNE CEDEX

EVALUATION OF HIGH TEMPERATURE MECHANICAL PROPERTIES AND CONSTITUTIVE EQUATION OF AUSTENITIC STAINLESS STEELS

P. BLANCHARD and J. TORTEL

Departement de Technologie / SRMA

SUMMARY

A large amount of experimental data (tensile tests, creep tests, cyclic strain tests, relaxation experiments and biaxial experiments) on 17-12 Mo SPH (316 L SPH) stainless steel have been obtained during the last years.

The aim of this paper is to illustrate by a few examples the work done in the constitutive equations area using this powerful data base.

I Numerous semiempirical equations have been developped to represent tensile, cyclic, creep or relaxation tests on 17-12 Mo SPH (316 L SPH) stainless steel. These equations, althrough not being able to be properly called "constitutive equations" in the full sense of the word, are nevertheless very useful for design studies. Actually these semiempirical equations are necessary tools for building elastic analysis's rules. Some examples of these equations are given along with specific applications (creep-fatigue rules).

II The qualitative and semiquantitative comparisons of the stress-strain behaviour (both uniaxial and biaxial) predicted by the most common constitutive equations (PRAGER, MEIJERS, HART, CHABOCHE, KRIEB, MILLER, ROBINSON) with the actual behaviour of 17-12 Mo SPH (316 L SPH) steel, allows us to shed some light on the strengths and weaknesses of these equations.

This comparison is presented and discussed. The way to more realistic equations is shown.

A detailed and quantitative comparison of the capabilities of two models, the CHABOCHE model and the multilayer unified model which has been developped at SRMA as a result of the preceeding discussion, is presented.

CONTENTS

1. INTRODUCTION

Designers must assess if the components they are investigating will withstand the loads that will be applied to them. To do this job, they need to calculate the stress and strain fields arising from these loads. Then two ways meet them : they can either assume that the components are build with an elastic and isotropic material, or suppose that generated stresses and strains meet a certain constitutive equation at least valid for one type of applied loading. In both cases, they need to know some mechanical properties of the materials the use of which is considered by them, to use them either alone or combined as limits or corrections in the elastic analysis design rules, or as data to assess and validate the constitutive equation they are using.

For this purpose, a large amount of experimental data (from tensile tests, creep tests, cyclic strain tests, relaxation and biaxial experiments) on the 17 12 Mo SPH (316 L SPH) stainless steel used for building the primary loop of the SUPER PHENIX 1 nuclear reactor, has been obtained in FRANCE during the last years. A general data base on the mechanical properties of this steel has been established.

The aim of this paper is at illustrating by some examples the work done using this powerful data base in the two areas of "classical" mechanical properties, and constitutive equations.

2. DEVELOPMENT OF SEMI-EMPIRICAL EQUATIONS DESCRIBING MATERIALS CHARACTERISTICS FOR ELASTIC ANALYSIS

2.1. INTRODUCTION

The mechanical characteristics of the Super-Phenix 1 nuclear reactor primary loop steel, AFNOR nitrogen controlled Z2 CND 17-12 (AISI 316 LN) grade are considered.

Numerous semi-empirical equations have been developped to represent tensile, cyclic, creep or relaxation tests on these S.S. . These equations, although not being appropriately called "constitutive equations" in the full sense of the word, are nevertheless very useful for design studies.

Actually, these semiempirical equations are necessary tools for using elastic analysis rules. Some examples of these equations along with specific applications are given below.

Experimental works for verifying an already prescribed equation are sometimes needed, an example of which is given below. In the following paragraphs, the subject is limited to the material characteristics and elastic analysis rules of the draft [1] , in which the considered steel form part of the grades and products having the characteristics 1S of part I - volume Z : technical appendix A3.

2.2. ASSESSMENT OR CHECKING OF MECHANICAL CHARACTERISTIC EQUATIONS

First, characteristics calling out one kind of properties : tensile or creep or fatigue properties are dealt with, then, those calling out two kinds of properties : tensile and creep properties, and detailed indications on establishing these characteristics are given. At last a characteristic calling out three kinds of properties : tensile, creep and relaxation properties, is considered and details on an experimental verification of the model of the relaxation calculus used to establish this characteristic, are given.

The description of the equation establishment or verification is preceded if necessary by a short presentation of the characteristic and always by an example of use of the characteristic in the elastic analysis rules. The following presentation is not intended to be exhaustive with regard to the characteristics used in [1] and the example of use of each characteristic in the rules is only shortly described.

2.2.1. Characteristics calling out only one kind of property

2.2.1.1. Tensile properties

2.2.1.1.1. YOUNG's modulus.

This datum is used to compute strain fields.

Its formulation is wholly used in [1] .

The experimental data plotted against temperature are within the scatter band of other steel grades data, especially the Phenix reactor main vessel

steel (see fig. 2.1.). Therefore the chosen mean equation is the one established with these other grades data, that is to say :

$$E = 194{,}000 - 81.4\ \theta$$

where E : YOUNG's modulus, in MPa, and θ : temperature in °C.

2.2.1.1.2. Time independent allowable stress.

This datum, referred to by S_m, is used to limit the equivalent primary membrane general stress when creep is negligible.

Its formulation is wholly used in [1] .

S_m is calculated from the minimum. 2 % proof stress : $R_{.002}$ and the minimum ultimate tensile stress : R_m according to :

$$S_m = \min \begin{cases} (1/3)\ R_m \text{ specified at } 20°C : R_m \geq 525 \text{ MPa} \\ (2/3)\ R_{.002} \text{ specified at } 20°C : R_{.002} \geq 220 \text{ MPa} \\ (1/2.7)\ R_m\ (\theta) \\ .9\ R_{.002}(\theta) \end{cases}$$

Here we limit ourselves to describing the formulation of mean and minimum $R_{.002}$. A similar description related to mean and minimum R_m could be made.

The products widely documented at temperature consist of three plates (F6, S7 and V8) and forged bars.

The variations of plates and bars $R_{.002}$ values against temperature are somewhat different and the bars $R_{.002}$ values make up the grade minimum values in their measurement temperature range, that is to say from 20°C to 600°C.

The following method of obtaining the law of variation of $R_{.002}$ against temperature for all the products, is chosen :

- the mean law of variation $R_{.002} = f(\theta)$ for the plates is determined by fitting a cubic to the whole of the plates experimental data obtained from 20°C

to 900°C (tensile strain rate : 1.7 % x min^{-1}) from which $R_{.002}$ (20°C) and the law normalized at 20°C are deduced :

$$R_{.002}(\theta) \; / \; R_{.002} \; (20°C) = g_1 \; (\theta)$$

- the bars mean variation law $R_{.002} = f \; (\theta)$ is determined by fitting a cubic to the whole of the bars experimental data, from which $R_{.002}$ (20°C) and the law normalized at 20°C are deduced :

$$R_{.002} \; (\theta) \; / \; R_{.002} \; (20°C) = g_2 \; (\theta)$$

- the grade mean law normalized at 20°C is determined from the ones of the bars and plates by fitting a cubic to computed data from $g_1(\theta)$ and g_2 (θ) at temperatures regularly distributed and identical in the measurement temperature range common to the plates and bars, from which the law normalized at 20°C is deduced :

$$R_{.002} \; (\theta) \; / \; R_{.002} \; (20°C) = g(\theta)$$

- the grade mean and minimum values at 20°C are determined :

. $(R_{.002})_{mean}$ = equally weighted mean of :

$(R_{.002})_{mean}$ of plates 15 to 60 mm thick (Super Phenix 1 nuclear reactor thickness range) including S6, F7 and V8 plates

$(R_{.002})_{mean}$ of bars

$(R_{.002})_{mean}$ of long products

that is to say :

$$(R_{.002})_{mean} \; (20°C) = 275 \text{ MPa}$$

. $(R_{.002})_{min}$ = $(R_{.002})_{min}$ specified at 20°C for the Super Phenix 1 nuclear reactor

that is to say :

$$(R_{.002})_{min} \; (20°C) = 220 \text{ MPa}$$

(actually the specified value for some products is now 210 MPa).

- the grade mean and minimum values at temperature are determined :

. $(R_{.002})_{mean}(\theta) = 275 \times g(\theta)$

that is to say :

$$(R_{.002})_{mean}(\theta) = 275 \times (1.0453 - 2.5053 \times 10^{-3}\,\theta + 4.1763 \times 10^{-6}\,\theta^2 - 2.5069 \times 10^{-9}\,\theta^3)$$

. $(R_{.002})_{min}(\theta) = 220 \times g(\theta)$

that is to say :

$$(R_{.002})_{min}(\theta) = .8 \times (R_{.002})_{mean}(\theta)$$

Figure 2.2 represents the whole of the experimental data and the computed mean and minimum curves.

2.2.1.2. Creep properties

2.2.1.2.1. Minimum creep rupture stress.

This stress, referred to by S_r, is used to compute the (creep) rupture use factor (creep rupture "damage") for creep-fatigue evaluation. Its formulation is only partly used in [1], according to time and temperature ranges.

Experimental data obtained on plates, bars and rods from 550°C to 700°C are represented in terms of a time-temperature equivalence parameter by an equation the form of which is :

$$\log_{10}(\sigma_{R\ mean}) = f(P)$$

where $P = (\theta + 273) \times (C + \log_{10} t)$ (LARSON and MILLER's parameter)

θ : temperature, in °C

t : time, in h

C : constant to be fitted.

More precisely, the following method is applied :

- a cubic with P variable is fitted and C value in P is adjusted to the whole of experimental data, from which a first mean curve is obtained

- a new set of data is made up comprising :

  . regularly distributed points on the first mean curve
  . mean UTS values at 550°C and 600°C associated with t = .1h

- a cubic is fitted to the new set of data.

The following equation is obtained :

$$\log_{10} (\sigma_{R\ mean}) = - 6.8923 + 1.4187 \times 10^{-3} P - 6.6217 \times 10^{-8} P^2 + 9.2370 \times 10^{-13} P^3$$

where $P = (\theta + 273) \times (20 + \log_{10} t)$

t in h, θ in °C and $\sigma_{R\ mean}$ in MPa.

This equation can be used in the following ranges :

$18,000 \leq P \leq 25,000$ $\qquad$ $525 \leq \theta(°C) \leq 700$

Figure 2.3 represents the variation of σ_R in terms of time in the form of isothermal curves.

The minimum rupture stresses are computed by the equation :

$$S_r = .8 \times \sigma_{R\ mean}$$

The lowest experimental points in the (P, $\log_{10} \sigma_R$) diagram are checked to be on the $\log_{10} S_r = f(P)$ curve.

2.2.1.2.2. Creep strains.

Creep strains ε_f depend on temperature, time and stress. Their formulation is used to estimate the increase by creep straining of the equivalent strain range already increased by plastic straining, in creep-fatigue evaluation.

The formulations presented in this paragraph are wholly used in [1] .

They concern small creep strains (primary and secondary creep) and are established with experimental date on three plates.

The primary creep law is obtained by fitting the following equation to experimental data obtained at a given temperature :

$$\varepsilon_f = C_1(\theta) \times t^{C_2(\theta)} \times \sigma^{n_1(\theta)}$$

where θ : temperature, t : time, and σ : stress.

The use of this formula is limited as follows :

- $\varepsilon_f \leq 1$ % and $550°C \leq \theta \leq 700°C$
- end of primary creep given by the condition of equality of primary to secondary creep rates.

For example, the following C_1, C_2 and n_1 values are obtained :

- at 550°C : $C_1 = 2.9618 \times 10^{-12}$, $C_2 = .42131$, $n_1 = 4.1800$
- at 700°C : $C_1 = 5.2375 \times 10^{-13}$, $C_2 = .80174$, $n_1 = 5.3313$

where ε_f is in %, t in h and σ in MPa.

Secondary creep is assessed by fitting NORTON's formula to secondary creep rate experimental data at a given temperature :

$$\dot{\varepsilon}_S = 100 \times C(\theta) \times \sigma^{n(\theta)}$$

where $\dot{\varepsilon}_S$ = secondary creep rate.

The use of this formula is limited as follows :

$$\dot{\varepsilon}_S \leq 10^{-2} \text{ \%} \times h^{-1} \quad \text{and} \quad 550°C \leq \theta \leq 700°C$$

For example, the following C and n values are obtained :

- at 550°C : $C = 5.29 \times 10^{-26}$, $n = 3.2$
- at 700°C : $C = 3.082 \times 10^{-18}$, $n = 6.72$

where $\dot{\varepsilon}_S$ is in % x h^{-1} and σ in MPa.

The following form of primary creep duration :

$$t_{fp} = C_3(\theta) \times \sigma^{n_3(\theta)}$$

and the following secondary creep formula :

$$\varepsilon_f = \varepsilon_{ffp} - \dot{\varepsilon}_S \times t_{fp} + \dot{\varepsilon}_S \times t$$

result from the foregoing, where ε_{ffp} : creep strain at the end of primary creep.

ε_{ffp} is calculated with the formula :

$$\varepsilon_{ffp} = C_1 \times C_3^{C_2} \times \sigma^{n_3 \times C_2 + n_1}$$

it depends on θ and σ.

Figure 2.4 shows two examples of the described fitting, for ε_f = .2 % and ε_f = .5 %, in the form of isothermal curves.

2.2.1.3. Fatigue properties

2.2.1.3.1. Cyclic curves.

These curves represent the variation of the total strain range, $\Delta\varepsilon_T$, in terms of the stress range, $\Delta\sigma$, at a given temperature. They are obtained from push-pull total strain-controlled fatigue tests and the stress range is obtained at a number of cycles equal to half the number of cycles to rupture.

These curves are used to estimate the increase by plastic straining of the equivalent strain range, in creep-fatigue evaluation. The curves presented in this paragraph are wholly used in [1] .

They were obtained in the plastic low-cycle fatigue field and in the temperature range from 20°C to 700°C on four AFNOR Z4 CND 18-12 (AISI 316) steel plates and five nitrogen controlled AFNOR Z2 CND 17-12 (AISI 316 LN) steel plates.

The method of establishing these curves includes the following steps :

- The strains are divided : $\Delta\varepsilon_T$ is fixed and measured during the test, the elastic strain range $\Delta\varepsilon_e$ is calculated from $\Delta\sigma$ with HOOKE's law, and the plastic strain range $\Delta\varepsilon_p$ is obtained by subtracting $\Delta\varepsilon_e$ from $\Delta\varepsilon_T$.

- The equation

$$\sigma_a = K'(\theta) \times \varepsilon_{pa}^{\ n'(\theta)}$$

where $\sigma_a = \frac{\Delta\sigma}{2}$ and $\varepsilon_{pa} = \frac{\Delta\varepsilon_p}{2}$, is fitted to the experimental data obtained on the whole of the products, at a given temperature.

- The curve

$$\sigma_a = f(\varepsilon_{ta})$$

where $\varepsilon_{ta} = \frac{\Delta\varepsilon_T}{2}$ is constructed : at a given value of σ_a, ε_{ta} is calculated by adding ε_{pa}, computed with the above fitted equation, to $\varepsilon_{ea} = \frac{\sigma_a}{E}$.

The formulation of E, used in the above calculations, has been given earlier.

For example, the following K' and n' values are obtained on the whole of the products :

- at 20°C : K' = 503 , n' = .343
- at 550°C : K' = 463 , n' = .326

where ε_{pa} is in %, and σ_a in MPa.

For example, figures 2.5a and 2.5b show the curves obtained at 20°C and 550°C on the whole of the products.

2.2.1.3.2. Fatigue curves (without hold time).

These curves give the allowable number of cycles N in terms of the strain range loading $\overline{\Delta\varepsilon}$ at a given temperature. They are used to assess the fatigue use factor (fatigue "damage"). Their formulation is only partly used in [1] , according to $\overline{\Delta\varepsilon}$ and temperature values.

These curves were obtained in the same fatigue field and temperature range and on the same products than cyclic curves.

Using the notations related to cyclic curves, the method of establishing these curves includes the following steps :

- the strains are divided : this step is identical to the one for cyclic curves
- the equation :

$$\Delta\varepsilon_p = C_p \times N_R^{-m}$$

where N_R : number of cycles to failure, is fitted to $\Delta\varepsilon_p$ experimental values obtained on the whole of the products at a given temperature

- the equation

$$\Delta\varepsilon_e = C_e \times N_R^{-p}$$

is fitted to $\Delta\varepsilon_e$ experimental values obtained on the whole of the products at a given temperature

- mean fatigue strength curves :

$$\Delta\varepsilon_t = f(N_R)$$

are constructed, where $\Delta\varepsilon_t$ is calculated from $\Delta\varepsilon_p$ and $\Delta\varepsilon_e$ values computed with the above equations, according to :

$$\Delta\varepsilon_t = \Delta\varepsilon_p + \Delta\varepsilon_e$$

- design curves :

$$\overline{\Delta\varepsilon} = f(N)$$

are assessed from mean curves as minimum curves in terms of N and $\overline{\Delta\varepsilon}$ among the following two :

$$\frac{N_R}{20} = f(\Delta\varepsilon_t) \qquad \text{and} \qquad N_R = f\left(\frac{\Delta\varepsilon_t}{2}\right)$$

For example, the following values are obtained for the whole of the products :

- at 20°C : $C_p = 28.5$, $m = .421$, $C_e = 1.35$, $p = .144$
- at 550°C: $C_p = 24.0$, $m = .485$, $C_e = 1.45$, $p = .162$

where $\Delta\varepsilon_p$, $\Delta\varepsilon_e$ and $\Delta\varepsilon_t$ are in %.

For example, figure 2.6 shows mean fatigue strength curves at 20°C and 550°C for the whole of the products.

2.2.2. Characteristics calling out several kinds of properties

2.2.2.1. Characteristics calling out two kinds of properties : tensile and creep properties

Here, we limit ourselves to considering the time-dependent allowable stress. This stress, referred to by S_t, is used to assess the creep use factor (creep "damage"). The latter is used for limiting the membrane primary general stresses when creep is significant.

S_t is assessed according to the following criteria :

$$S_t = \min \begin{cases} \sigma_{1\ \%\ \text{total min}} \\ .8 \times \sigma_{fs.2\ \text{min}} \\ (2/3) \times S_r \end{cases}$$

where $\sigma_{1\ \%\ \text{total min}}$: minimum stress bringing about 1 % total (elastic + plastic + creep) strain, and

$\sigma_{fs.2\ \text{min}}$: minimum stress bringing about .2 % offset secondary creep end.

S_r formulation is given above.
As the latter is only partly used in [1] , it's just the same for S_t one, though $\sigma_{fs.2\ \text{min}}$ and $\sigma_{1\ \%\ \text{total min}}$ formulations are wholly used in [1] .

$\sigma_{fs.2\ \text{min}}$ formulation is similar to S_r one, so it is not described here.

$\sigma_{1\%\ \text{total min}}$ formulation includes the following steps :

2.2.2.1.1. The mean isochronous curves are constructed.

These are the curves :

$$\sigma = f(\varepsilon_T)$$

at given temperature θ and time t

where ε_T : total strain, and σ: stress. ε_T is calculated at given σ, t and θ , with the equation :

$$\varepsilon_T (\sigma, t, \theta) = \varepsilon_e (\sigma, \theta) + \varepsilon_p (\sigma, \theta) + \varepsilon_f (\sigma, t, \theta)$$

with ε_e : elastic strain computed with HOOKE's law and YOUNG's modulus formula given earlier

ε_p : plastic tensile strain

ε_f : creep strain the formulas of which were given earlier.

During a tensile test :

$$\varepsilon_T(\sigma, \theta) = \varepsilon_e (\sigma, \theta) + \varepsilon_p (\sigma, \theta)$$

ε_p formulation

Tensile tests on two plates at temperatures from 20°C to 1200°C - a number of them were run to rupture - were analyzed at a given temperature, using the equation :

$$\frac{\sigma}{R_{.002}} = C \times \varepsilon_p^n$$

where ε_p and σ are true strain and stress, and C and n coefficients may vary in terms of ε_p range.

Figures 2.7a and b show the variation of C and n coefficients in terms of temperature, in the range $\varepsilon_p \leq 1$ %.

We limit ourselves to :

$$\varepsilon_p \leq 1\ \% \quad , \quad 20°C \leq \theta \leq 700°C$$

In that case :

$$\sigma = (R_{.002})_{mean} (\theta) \times 1.17 \times \varepsilon_p^{.096}$$

where ε_p is in %, σ is in MPa and $(R_{.002})_{mean} (\theta)$ was given earlier.

The isochronous curves are drawn from 550°C to 700°C for durations up to 3×10^5 h. ε_f is extrapolated for durations longer than 10^4h. ε_T is limited by the condition $\varepsilon_p \leq 1$ %.

2.2.2.1.2. The $\sigma_{1\ \%\ \text{total mean}}$ stresses are determined.

They are determined on the isochronous curves at a given temperature and a given duration, the maximum duration being limited to 10^4 h.

2.2.2.1.3. The formulas giving $\sigma_{1\ \%\ \text{total}}$ stresses are worked out.

The values of $\sigma_{1\ \%\ \text{total mean}}$ obtained above are represented in terms of an equivalence (t,θ) parameter by an equation the form of which is :

$$\log_{10} (\sigma_{1\ \%\ \text{total mean}}) = f\ (P)$$

where : $P = (\theta + 273) \times (C + \log_{10} t)$ (LARSON and MILLER's parameter) and f is a third degree polynomial, and this polynomial and the value of C in P are both fitted to the whole of the stress values.

Figure 2.8 represents the variation of $\sigma_{1\ \%\ \text{total mean}}$ in terms of time in the form of isothermal curves.

Minimum values of $\sigma_{1\ \%\ \text{total}}$ stresses, which are required for S_t calculation, are computed with :

$$\sigma_{1\%\ \text{total min}} = .8 \times \sigma_{1\ \%\ \text{total mean}}$$

2.2.2.2. Characteristics calling out three kinds of properties : tensile, creep and stress relaxation properties

Here, we limit ourselves to considering the unsignificant creep curve. It's a time-temperature decreasing curve which divides the time-temperature field into two regions : the significant creep region (region of long durations or high temperatures) and the unsignificant creep one.

This curve is assessed according to the following method, applied at a given temperature :

- S_m and E are calculated with the formulas given earlier,

- the $\frac{3 \times S_m}{E}$ strain, then the stress σ_o corresponding to this strain on the mean tensile curve the formulation of which was given in the paragraph devoted to S_t, are calculated

- the stress relaxation duration from σ_o at constant total strain, corresponding to the value .1 of the ratio of the relaxed stress $\Delta\sigma$ to σ_o is calculated. The relaxation calculus assumptions are the following ones :

  . creep strain (under constant stress) complies with the formula :

$$\varepsilon_f = C_1 \times t^{C_2} \times \sigma^{n_1}$$

  . creep strain rates $\frac{d\varepsilon_f}{dt}$ during the stress relaxation and under constant stress are equal if stresses and durations are equal (time-hardening assumption, more conservative than strain hardening one).

The looked for relaxation duration is computed from :

$$t = \left[\frac{\frac{1}{(.9)^{n_1-1}} - 1}{E \times C_1 \times (n_1-1) \times \sigma_o^{n_1-1}} \right]^{\frac{1}{C_2}}$$

where $C_1(\theta)$, $C_2(\theta)$, $n_1(\theta)$ and $E(\theta)$ are given by formulations described earlier (σ_o is also a function of θ).

Therefore this formula represents a relation $t(\theta)$ which is the equation of the negligible creep looked for curve.

Relaxation tests and calculations on a plate at temperature from 550°C to 700°C were compared at given temperature and initial stress. The computations were done with the above assumptions and the tensile and creep properties of the tested plate. At a given temperature, among the test initial stresses, there was always one near the tested plate σ_o stress (calculated according to the above method).

For example, figure 2.9 shows the comparison between experimental data and calculated curves at 550°C and 700°C for initial stresses near plate σ_o stresses (for this plate : at 550°C : σ_o = 146 MPa ; at 700°C : σ_o = 133 MPa).

From the examination of the whole of the comparisons in the short experimental duration range (from 1 h to 10 h), it can be seen that the lack of conservatism of predicted relaxation duration at 550°C is progressively replaced by some conservatism at 700°C, the prediction being right at 650°C. However, the interesting durations corresponding to $\frac{\Delta\sigma}{\sigma_o} = .1$ are in the order of 1 h at 550°C and 600°C but much shorter than 1 h at 650°C and 700°C.

2.3. PRESENT WORK ON MECHANICAL CHARACTERISTICS

The following review is not exhaustive.

2.3.1. The work on the preparation of the numerous new tensile and creep data, in order to formulate tensile and creep characteristics again, is in progress. This formulation could replace the present one in a future issue of [1]

2.3.2. The following ones of many works on creep-fatigue evaluation may be pointed out :

2.3.2.1. Experimental assessment and checking of the "symmetrisation" factor $K_s = \sigma_{max}/\Delta\sigma$ applied in [1] to the equivalent stress range, where σ_{max} : maximum stress during the cycle. This factor is used to assess the stress used for calculating :

- the increase of the equivalent strain range by creep straining,
- the (creep) rupture use factor.

For example, figure 2.10 shows the variation of K_s values calculated with experimental data from uniaxial tests during which the strain was varied from 0 to a maximum fixed value, on a plate at 550°C and 600°C, in terms of

$$r = \frac{\Delta\sigma_{calc}}{2xR_{.002}} .$$

In this figure :

- $\Delta\sigma_{calc}$ is the grade stress range given earlier ($\Delta\sigma_{calc} < \Delta\sigma_{exp}$, after the stabilization of $\Delta\sigma_{exp}$ values)

- r is calculated with the plate $R_{.002}$ in the experimental points whereas

it is calculated with the grade $(R_{.002})_{min}$ given earlier, on the $K_s(r)$ curves

- the prestraining of the tested material consists exclusively in strain cycling from 0 to a maximum strain, at the same temperature and at a smaller total strain range, than during the following test.

2.3.2.2. (creep) rupture use factor assessment in the presence of compression stresses. Presently, this case is not distinguished from the one when there are tensile stresses only. Uniaxial comparative relaxation fatigue tests were done on a plate at 600°C, the stress relaxation occurring either at the maximum total tensile strain or at the maximum total compression strain.

Figure 2.11 shows the variation of the life reduction factor F_{R25} in terms of strain hold time and nature. In this figure :

$$- F_{R\ 25} = \frac{N_{25}\ (t_m)}{N_{25}\ (t_m = 0)}$$

where N_{25} : number of cycles corresponding to a 25 % decrease of the maximum tensile stress $\sigma_{t\ max}$ or of the maximum compression stress $\sigma_{c\ max}$ at the beginning of the hold time, compared with the maximum $\sigma_{t\ max}$ or $\sigma_{c\ max}$ values during the test,

t_m : strain hold duration

- $\Delta\varepsilon_t$ is the set total strain range.

It can be seen that the life reduction factor for long hold times is much smaller for compression hold times than for tensile ones. Therefore, the use of the same rupture use factor in the presence of compression stresses and without them seems to be a too conservative practice.

2.4. CONCLUSION

The above presentation constitutes a review of the formulation or checking of some characteristics of the 17-12 Mo SPH, used for the application of the design rules of [1] based on elastic analysis.

The use of some properties in several characteristics is worth noting.

With the exception of YOUNG's modulus, the properties used express the inelastic behaviour of the material and take part in characteristics themselves connected with design rules where they contribute to take account of this behaviour, whereas stresses and strains are elastically calculated.

ACKNOWLEDGMENTS

All the work presented in § 2 has been performed both at the CEA-IRDI-SRMA (SACLAY) metallurgical laboratories by Miss FELSEN's (previously Mr CALVET's) team (tensile, creep and stress relaxation properties) and Mr MOTTOT's team (stress cycle "symmetrisation" during unsymmetrical fixed strain cycling), and in the framework of the EDF-CEA agreement related to the R. and D. for the FBR line, Materials Task Force (fatigue and compression creep-fatigue properties). It has resulted in restricted distribution papers only.

3. CONSTITUTIVE MODELLING OF 17-12 Mo SPH STAINLESS STEEL BEHAVIOUR AT HIGH TEMPERATURE

The following points are addressed in this chapter :

3.1. Overview of the key features of 17-12 Mo SPH stainless steel inelastic behaviour at high temperature ;

3.2. Qualitative and semi-quantitative comparisons of the stress/strain behaviour (both uniaxial and biaxial behaviour) predicted, for three typical loadings, by the current constitutive equations with the actual behaviour under these loadings ;

3.3. Physical basis of the unified multilayer model ;

3.4. Identification method of the unified multilayer model ;

3.5. Comparison with the elastoplastic CHABOCHE model ;

3.6. Conclusion.

The litterature references pertaining to the multilayer unified model are :

- [2] to [6] : works of the founding fathers of the multilayer model ;
- [7] : work of the I.M.G. GRENOBLE on the discrete memory hereditary type model (rigorous generalizing of the multilayer model) ;
- [8] to [14] : recent theoretical and experimental studies ;
- [15] to [17] : creep studies ;
- [18] to [24] : current constitutive equations (others than multilayer models).

3.1. OVERVIEW OF THE KEY FEATURES OF 17-12 Mo SPH STAINLESS STEEL INELASTIC BEHAVIOUR AT HIGH TEMPERATURE

The following features have been selected as typical of the inelastic behaviour of 17-12 Mo SPH S.S. at high temperature :

1) hardening is non linear in a monotonic or cyclic tensile test ;

2) cyclic and monotonic uniaxial strain/stress curves are nearly homothetical within a factor of two (Masing behaviour) when cyclic hardening is stable ;

3) for small enough strain amplitudes plastic shakedown is reached after a few tens of cycles in a ratchet experiment ;

4) for large enough strain amplitudes progressive distortion (constant rate ratchetting) does develop at high temperatures ;

5) progressive distortion is linked with the effect of time on inelastic strain ;

6) progressive distortion is possible at high temperature (where creep is significant), it is impossible at 300°C where creep is not significant ;

7) in a ratchet experiment, every increase of the cyclic strain entails a new wave of ratchet strain (even after plastic shake down) ;

8) in a ratchet experiment, every decrease of the primary stress entails a decrease of the inelastic strain in the primary stress direction (negative ratchet) ;

9) the two apparent categories of inelastic strain ("plastic strain" and "creep strain") do interact : the increase of the hold time at a cycle extremum entails a higher relaxation strain at this point and a higher plastic strain in the following half cycle.

3.2. QUALITATIVE AND SEMI-QUANTITATIVE COMPARISONS OF THE STRESS/STRAIN BEHAVIOUR PREDICTED FOR THREE TYPICAL LOADINGS, BY THE CURRENT CONSTITUTIVE EQUATIONS, WITH THE ACTUAL BEHAVIOUR UNDER THESE LOADINGS

In this paragraph three particular loadings have been selected as typical of some important situations encountered in LMFBR development.

For these loadings the actual behaviour of 17-12 Mo SPH S.S. at high temperature is compared with the predicted behaviour according to each of the constitutive equations set. In order to simplify the discussion we assume that there is no large variation of the cyclic hardening during the test, the most important feature of the constitutive equations being,

according to us, the evolution law of the center of the yield surface (or the center of the equipotential surfaces). As we shall see below, this law governs the ability of the model to adequately (or not) predict the actual behaviour of the material.

3.2.1. Monotonic tensile test

Is the model able to predict the experimentally observed non linear hardening ?

Obviously it is not the case with the PRAGER model and almost obviously with the KRIEG model (when the strain rate is low and the recovery is negligible). For all the other models, $d\varepsilon_p$ being a non linear function of dX, a non linear hardening is predicted by the model.

3.2.2. Uniaxial cyclic test where the stress is cycled in the $(0,\sigma)$ interval

Is the model consistent with the actual behaviour : either progressive distortion or plastic shakedown according to the stress range ?

- The PRAGER model, being a linear kinematic model, is consistent with elastic or plastic shakedown. It does not predict any progressive distortion.

- The MEIJERS model, being (after stabilization of the cyclic hardening) an elastic-ideally plastic multilayer model is able to predict either progressive distortion or plastic shakedown according to the stress amplitude.

- The HART model, being an isotropic hardening model, does not allow progressive distortion.

- The CHABOCHE model, including an evanescent memory term $\dot{p}\,\tilde{X}_n$ in its evolution law $\dot{\tilde{X}}_n = C_n\,(a_n\,\dot{\tilde{\varepsilon}}_p - p\,\tilde{X}_n)$, does not allow plastic shakedown.

- The KRIEG, MILLER and ROBINSON models all three do predict both plastic shakedown for small enough stress ranges and time dependant progressive distortion for large enough stress ranges, because the evolution laws of these three models include a recovery term which is both time dependant and strongly dependant on the second invariant of the internal stress $\tilde{X}$. (Our own model includes this important character).

3.2.3. Tension/torsion of a tube with constant axial stress and constant cyclic torsion amplitude

Is the model consistent with the following experimental fact : a new wave of progressive distortion arises when the cyclic torsion amplitude increases (after having reached the plastic shakedown) ?

- The PRAGER model is not consistent with this behaviour because $\sigma_{XX} = X_{XX}$ after plastic shakedown. Therefore the asymptotic level of $\varepsilon_{p\ XX}$ is not dependent on $\Delta\varepsilon_{xy}$;

- The MEIJERS model, being a multilayer model, allows an increase of progressive distortion with the torsion strain amplitude ;

- The HART model, being an isotropic hardening model, is consistent with a new wave of progressive distortion as the cyclic torsion amplitude increases ;

- The CHABOCHE model too predicts the actual behaviour : its evanescent memory term implies a tensile strain increment for each increase of the torsion strain ;

- The KRIEG, MILLER and ROBINSON models, being all three models with only one layer and no erasing of memory by strain, do not allow a new wave of progressive distortion to appear when the cyclic torsion amplitude increases. This impossibility is due to the fact that, after shake down, $\sigma_{XX} = X_{XX}$ exactly as with the PRAGER model.

3.3. PHYSICAL BASIS OF THE UNIFIED MULTILAYER MODEL

This model has been built to represent

1) the strain's and hardening's heterogeneities in the substructure,
2) the recovery at high temperature.

3.3.1. The influence of strain's and hardening's heterogeneities on the deformation of a polycristal is rather well known and has been better experimentally studied and more accurately modelled during the last years.

3.3.2. The hardening is assumed to be of the PRAGER linear type in each of the layers of the multilayer "sandwich". This assumption is intended to represent the small strain plastic behaviour of each subgrain in a polycristal of constant or nearly constant substructure (and therefore of constant or nearly constant cyclic hardening).

This kinematical hardening allows in this way to model the BAUSHINGER effect in each subgrain (or more generally in each constant hardness region of the metal).

3.3.3. The recovery is assumed to be governed by diffusion and therefore to be time dependant (as it is usually the case for creep controlled by dislocation climb). This recovery is assumed to leave unmodified the substructure (walls, subboundaries modelled by isotropic hardening) and therefore to affect only the back stresses of subboundaries and dislocations bows, or pileups (modelled by the Kinematical hardening).

3.3.4. The fundamental equation (evolution law) modelling the classical hardening-recovery balance is therefore

$$\dot{X}_{hk_i} = a_i \dot{\varepsilon}^p_{hk_i} - K J_2 (X_i)^{n-1} X_{hk_i} \qquad (1)$$

in the i layer.

This being valid for low strain and the 300-700°C temperature range.

The total (inelastic plus elastic) strain is assumed to be the same in all the layers.

3.4. METHOD OF IDENTIFICATION

3.4.1. Uniaxial experiments

There is no unique way to identify a multilayer model using the tensile curve : actually there is an infinity of ways of doing this. In the identification choice the only constraint is the following : α_i being the weight of the i layer and a_i being the kinematic hardening coefficient of this layer, it can be proved that

$$\frac{E \ \Sigma\alpha_i a_i}{E + \Sigma\alpha_i a_i}$$

is inferior to the slope π of the tangent to the rational tensile curve (either at the end point of this curve or at the point of maximal strain on this curve).

The tensile curve obtained with this model (identification with ten layers) is presented in fig. (3.1) along with the RCC-MR tensile curve on which the identification has been carried out.

From now on the same identification is used in all the figures of this report. In this identification all the layers are assumed to have the same Young modulus : the Young modulus E of the bulk polycristalline aggregate. This seems to be a sensible assumption since it is thought that the plastic anisotropy of the various metal areas is not statistically linked with their elastic anisotropy.

A further constraint is imposed on the K_i coefficients which are the material sensitive coefficients in the uniaxial recovery rate equation

$$\dot{X}_i = - K_i \ I_2 \ (x_i)^{n-1} \ X_i \qquad (2)$$

all the K_i coefficients are assumed to be equal. This constraint results from the above hypothesis according to which the recovery rate being controlled by dislocation climb, therefore by diffusion, it does not depend directly on the particular area of the metal where it is taking place.

One can prove that the K coefficient is linked with the secondary creep rate $\dot{\varepsilon}$ and with the two quantities $\Sigma\alpha_i a_i^{1/n}$ and $\Sigma\alpha_i R_i$ (which both depend only on the distribution of the slopes a_i in the various layers i) by equation :

$$k = \dot{\varepsilon} \ \left(\frac{\Sigma \ \varepsilon_i \ a_i^{1/n}}{\sigma - \Sigma\alpha_i \ R_i} \right)^n \qquad (3)$$

(R_i being the radius of the yield surface of the layer i).

The identification is carried out along the following lines :

- first step : the tensile-torsion tests allow to reach the distribution of the a_i coefficients ;

- second step : the distribution of the yield surfaces radii R_i is derived (on purely mathematical ground) from the distribution of the a_i coefficients and from the tensile curve (this is carried out by a small computation program) ;

- third step : knowing the secondary creep rate $\dot{\varepsilon}_1$ and $\dot{\varepsilon}_2$ under two stresses σ_1 and σ_2 equation (3) allows to compute both n and K.

Fig. 3.2. shows the isochronous creep curves which have been calculated (at 650°C) by the integration method which is described in appendix 3.1.

3.4.2. Biaxial experiments - Experimental determination of the a_i distribution

The numerical integration method of the strain/stress equations is presented in appendix 3.2.

- The influence of the coefficients a_i on the ratchet strain, in experiments with constant tensile stress and constant torsion strain amplitude, is obvious on fig. (3.3) and (3.4) which show the evolution of the ratchet strain as a function of the number of cycles for two quite different distributions : the first distribution including only a_i of negligible values, the second distribution indluding some a_i of rather high value (10^4 and 5.10^4 MPa), the two distributions matching nevertheless the same tensile curve.

- The ideal identification method would be to carry out a serie of tensile/torsion tests under a constant tensile stress and with a low cyclic torsion amplitude, the tensile stress growing progressively from test to test.

This procedure would enable us to reach successively the plastic deformation of all the i layers. One could in this way exactly compute the distribution of the a_i coefficients. A full set of such experiments has not yet been performed. Nevertheless a first and rather good estimate

of this distribution has been derived from the available data : the ratchet strains at the end of the "primary phases" (where the ratchet strain per cycle decreases) in a serie of tensile/torsion tests carried out under low cyclic torsion amplitude (therefore with negligible cyclic hardening) and under various tensile stresses.

The consistency of the model is then checked : the ratchetting rate (increment of ratchett-strain per cycle) in the "secondary phase" of the ratchet experiment (phase where the ratchetting rate is constant) is numerically computed. Actually this rate is very similar to the experimental rate (fig. 3.5, 3.6 and 3.7).

Two facts have to be underlined here :

1) it is at the end of the "primary phase" of the ratchet experiment that the difference between the two computed ratchet strains (with and without recovery, with the same distribution of the a_i coefficients in each case) starts being non negligible (fig. 3.8) ;

2) at 300°C, temperature where the 17-12 Mo SPH creep and recovery rate is negligible, the ratchet strain reach an asymptotic constant value after a few tens of cycles.

Therefore no progressive distortion (infinite ratchetting) is observed (fig. 3.9) in clear opposition to the permanent ratchet rate which is manifest at 650°C.

In this paragraph we have numerically assessed the clear link between creep (or recovery) and progressive distortion, link which had been previously experimentally assessed.

3.4.3. Discussion

Does the multilayer unified model still have some degrees of freedom when the above described identification procedure has been fullfilled ?

The answer to this question is yes if it is noticed that the result of the identification is not strongly dependent on the presence (or on

the absence) of a small proportion of hard layers (i.e. of layers of high a_i coefficients) (figure 3.10).From a metallurgical point of view the presence of such hard layers is not an unrealistic assumption : they might correspond to the hard walls whose role in creep is thought to be important by electron microscopists.

Besides, such a presence of a small proportion of hard layers allows to model quite accurately the primary creep (fig. 3.11).

Nevertheless it seems unrealistic to rely entirely on recovery for modelling the effect of time on the inelastic strain in 17-12 Mo SPH SS and to ignore the contribution of a viscous mechanism in fast transients.

Such a viscous mechanism is taken into account in a viscoplastic generalization of the present model which is beyond the scope of this paper.

3.5. COMPARISON OF THE UNIFIED MULTILAYER MODEL WITH THE CHABOCHE ELASTOPLASTIC MODEL

We recently proposed a method which enables us to identify the five parameters CHABOCHE elastoplastic model by using three points of the stress-strain cycle (of constant cyclic hardening). This method can lead to two quite different sets of five coefficients (a_1C_1 a_1C_2 R), both sets allowing nevertheless a rather accurate modelling of the same cycle (fig. 3.12 and 3.13). In this way we succeeded in varying the C_2 coefficient in the (3.10^3 to 1.10^{-5}) interval without neither modifying the (ε,σ) cycle representation nor suppressing the "oversquare" character of the (ε_{xx}, σ_{xy}) ratchet curve in a numerical biaxial experiment (fig. 3.14 to 3.17).

This "oversquare" character is typical of the biaxial numerical experiments carried out with the CHABOCHE elastoplastic model and would still be present with a larger number of parameters.

A second discrepancy between the CHABOCHE model and the experimental results is the plastic shakedown which this model is able to model adequately only in one case : when one of the C_1 or C_2 coefficient is very small (here 10^{-5}). Unfortunately the selection of such a particular value

for C_2 would lead the CHABOCHE model to two new discrepancies with the experimental facts : the calculated ratchet strain would be no longer dependant on the strain range (which is quite unrealistic) and would be a linear function of the primary axial stress (which is not realistic either).

The unified multilayer model does not present this anomaly (fig. 3.18a and 3.18b).

3.6. CONCLUSION

1) The unified multilayer model allows an adequate constitutive modelling of

- the uniaxial tensile tests results,
- the uniaxial creep tests,
- the biaxial tensile/torsion experiments

on the 17-12 Mo SPH stainless steel whose cyclic hardening can be considered as stable for practical purposes.

The very beginning of primary creep and of relaxation tests (fast transients) have now to be modelled with an extension of the present model. This extension should include a viscoplastic potential.

2) The CHABOCHE elastoplastic model does not allow an adequate modelling of the tensile/torsion ratchet experiments carried out on the same material.

ACKNOWLEDGMENTS

- The Scientific exchanges within the "GIS Rupture à CHAUD" group are also acknowledged as a very significant and stimulating help.

- We have to thank more particularly Mr P. COUSSERAN, J. LEBEY, G. CLEMENT, A. TREMBLAIS, P. CORBEL for authorizing us to use their unpublished tensile/torsion experimental data.

NOTATIONS

σ_{xxi}, σ_{xyi}	tensile and torsion stresses in the i layer
X_{xxi}, X_{xyi}	coordinates of the yield surfaces center of the i layer
R_i	radius of the yield surface of the i layer
ε^p_{xxi}, ε^p_{xyi}	inelastic tension and torsion strains of the i layer
ε_{xx}, ε_{xy}	total tension and torsion strains
a_i	kinematical hardening coefficient of the i layer
K	internal stresses recovery coefficient
E and μ	elastic Young and shear moduli

4. GENERAL CONCLUSION

Fast Breeder Reactors are designed to keep as low as possible the creep, fatigue and ratchetting damages in the structures, so, either elastic analysis or inelastic analysis has to be carried out in design studies.

This paper presents a short account of some 17-12 Mo SPH (316 LN) steel properties enabling the "codes and standards" specialists to build reliable elastic analysis rules and to propose realistic inelastic analysis equations.

GENERAL ACKNOWLEDGMENTS.-

Most of the work presented in this paper has been performed under the auspices of the AFCEN and the CEA-EDF-NOVATOME Comittee intended to develop rules for fast breeder reactor structures analysis.

REFERENCES

[1] Projet de règles de conception et de construction des matériels mécaniques des ilots nucléaires RNR (RCC-MR), association française pour les règles de conception et de construction des matériels des chaudières électronucléaires (AFCEN), provisional issue, december 1983

[2] G. MASING, Wiss. Veröff. Siemens-Werke 3, 231 (1923)

[3] J.F. BESSERLING, J. Appl. Mech. 25, 612 (1958)

[4] B. PERSOZ, "La Rhéologie", Masson, Paris (1969)

[5] P. MEIJERS, G.T.M. JANSSEN, J. BOOIJ, Numerical plasticity and creep analysis based on the fraction model, 3ème SMIRT, Londres (1975)

[6] W.D. IWAN, J. of Appl. Mech. 89, 612 (1967)

[7] B. WACK, J.M. TERRIEZ, P. GUELIN, Acta Mechanica 50, 9-37 (1983)

[8] C. HOLSTE, H. BURMEISTER, Physica Status Solidi(a) 269 (1980)

[9] J. POLAK, M. KRESNIL, Fatigue of Engineering Materials and Structures vol. 5, n°1, 19-56 (1982)

[10] H. MUGRABI, Acta Met., vol. 31, n° 9, 1367-1979 (1983)

[11] F. DOBES, Acta Met, vol. 28, 377-382 (1980)

[12] M.A. MORRIS, J.L. MARTIN, Acta Met, vol. 32, n° 4, 549-561 (1984)

[13] M.A. MORRIS, J.L. MARTIN, 2nd Intern. Conf. on Creep of eng. mat. & struct., Swansea, 103-114 (1984)

[14] H.P. LIEURADE, P. RABBE, L. ROESCH, Mem. Sci. Rev. Met. 59, n° 11, 815 (1972)

[15] B. WILSHIRE, Actes du Colloque IUTAM, Leicester, 72 (1980)

[16] R. LAGNEBORG, Met. Sci. J. 127 (1972)

[17] C.E. PUGH & D.N. ROBINSON, Nucl. Eng. Des., 269 (1978)

[18] C.G. SCHMIDT & A.K. MILLER, Res. Mechanica, 109 (1981)

[19] R.D. KRIEG, J.C. SWEARINGEN & R.W. RHODE, ASME, MPC7, 15

[20] F.A. LECKIE, Actes du colloque IUTAM, Leicester, 14 (1980)

[21] J.L. CHABOCHE & G. ROUSSELIER, Conference post SMIRT (1981)

[22] C. OYTANA, P. DELOBELLE, A. MERMET, J. of Eng.Mat.Tech., 1-11 (1982)

[23] C. EXCELLENT, J.BIROCHEAU,L. BORNIER, J.Mec.Theor.appl.3,n°3,371-380(1984)

APPENDIX 3.1

UNIFIED MULTILAYER MODEL

UNIAXIAL CREEP CALCULATIONS

PRIMARY CREEP

The equilibrium equation is :

(1) $$\sigma = \Sigma \alpha_i (R_i + X_i)$$

or by differentiating :

(2) $$0 = \Sigma \alpha_i \, dX_i$$

α_i being the weight of the layer i

R_i being the yield surface radius of the layer i.

The p-1 equations expressing the compatibility conditions in the p layers are :

(3) $$dX_1\left(\frac{1}{E} + \frac{1}{a_1}\right) + \frac{K}{a_1} X_1^n \, dt = \ldots\ldots = dX_i\left(\frac{1}{E} + \frac{1}{a_i}\right) + \frac{K}{a_i} X_i^n dt = \ldots = d\varepsilon$$

Since when each of the p layers is plastically deformed,

$$d\sigma_i = dX_i$$

$$d\varepsilon_{i\,\text{elastic}} = d\sigma_i / E = dX_i / E$$

$$d\varepsilon_{i\,\text{plastic}} = \frac{dX_i}{a_i} + \frac{K}{a_i} X_i^n dt$$

this leads to

(4) $$\Sigma \alpha_i \left(d\varepsilon - \frac{K}{a_i} X_i^n dt\right) \Big/ \left(\frac{1}{E} + \frac{1}{a_i}\right) = 0 \quad \text{or} \quad \frac{d\varepsilon}{dt} = K \frac{\Sigma \left[\frac{\alpha_i X_i^n}{a_i} \Big/ \left(\frac{1}{E} + \frac{1}{a_i}\right)\right]}{\Sigma \frac{\alpha_i}{1/E + 1/a_i}}$$

which allows to calculate $d\varepsilon/dt$; on the other hand the dX_i are derived from equation (3) :

$$dX_i = \left(d\varepsilon - \frac{K}{a_i} X_i^n dt\right) \Big/ \left(\frac{1}{E} + \frac{1}{a_i}\right)$$

SECONDARY CREEP

When the stationary regime is reached, then $dX_i = 0$ and the equation (3) leads to

$$(X_1/X_i)^n = a_1/a_i$$

and $$d\varepsilon/dt = \frac{K}{a_1} X_1^n$$

which leads to :

$$\sigma - \Sigma \alpha_i R_i = \Sigma \alpha_i X_i$$

$$= X_1 \left[\alpha_1 + \alpha_2 \left(\frac{a_2}{a_1}\right)^{\frac{1}{n}} + \ldots\ldots + \alpha_i \left(\frac{a_i}{a_1}\right)^{\frac{1}{n}} + \ldots\right]$$

$$= \left(\frac{a_1}{K} \frac{d\varepsilon}{dt}\right)^{\frac{1}{n}} \left[\alpha_1 + \alpha_2 \left(\frac{a_2}{a_1}\right)^{\frac{1}{n}} + \ldots\ldots + \alpha_i \left(\frac{a_i}{a_1}\right)^{\frac{1}{n}} + \ldots\ldots\right]$$

whence $$\sigma - \Sigma \alpha_i R_i = \left(\frac{1}{K} \frac{d\varepsilon}{dt}\right)^{\frac{1}{n}} \Sigma \alpha_i a_i^{\frac{1}{n}}$$

from which the expression of K can be derived :

$$K = \frac{d\varepsilon}{dt} \left(\frac{\Sigma \alpha_i a_i^{\frac{1}{n}}}{\sigma - \Sigma \alpha_i R_i}\right)^n$$

APPENDIX 3.2

UNIFIED MULTILAYER MODEL

INTEGRATION METHOD FOR A TENSILE/TORSION EXPERIMENT

UNDER CONSTANT AXIAL STRESS

Since the axial stress is constant

$$\sum \alpha_i \, d\sigma_{xx_i} = 0$$

α_i being the weight of the i layer.

A - EQUATIONS PERTAINING TO THE LAYERS WHERE THERE IS "PLASTIC DEFORMATION"

$$\text{if } J_2(\sigma_i - X_{i_0}) > R_i$$

(σ_i being the stress tensor in the i layer)
(x_{io} being the internal stress tensor at the last cycle extremum)
(R_i being the yield surface radius of the i layer).

A.1 - Equations expressing the evolution laws in these layers

$$(1) \quad dX_{xx_i} = a_i \, d\varepsilon^p_{xx_i} - K J_2(X_i)^{n-1} X_{xx_i} \, dt$$

$$(2) \quad dX_{xy_i} = a_i \, d\varepsilon^p_{xy_i} - K J_2(X_i)^{n-1} X_{xy_i} \, dt$$

replacing $d\varepsilon^p_{xx_i}$

by $d\varepsilon_{xx} - \frac{d\sigma_{xx_i}}{E}$

and $d\varepsilon^p_{xy_i}$

by $d\varepsilon_{xy} - \frac{d\sigma_{xy_i}}{2\mu}$

this leads to :

$$(3)\qquad \frac{dX_{xx_i}}{a_i} = d\varepsilon_{xx} - \frac{d\sigma_{xx_i}}{E} - \frac{k}{a_i} J_2(X_i)^{n-1} X_{xx_i}\, dt$$

$$(4)\qquad \frac{dX_{xy_i}}{a_i} = \frac{2}{3} d\varepsilon_{xy} - \frac{2}{3}\frac{d\sigma_{xy_i}}{2\mu} - \frac{k}{a_i} J_2(X_i)^{n-1} X_{xy_i}\, dt$$

A.2 - Equations expressing the normal flow rule in each of the layers where there is plastic deformation

$$d\varepsilon^{p}_{xx_i} / d\varepsilon^{p}_{xy_i} = 2(\sigma_{xx_i} - X_{xx_i}) / 3(\sigma_{xy_i} - X_{xy_i})$$

or taking into account equations (1) and (2)

$$\left(d_{xx_i}/a_i + k J_2(X_i)^{n-1} X_{xx_i}\, dt/a_i\right) / \left(3\, dX_{xy_i}/2a_i + 3k J_2(X_i)^{n-1} X_{xy_i}\, dt/2a_i\right) = 2(\sigma_{xx_i} - X_{xx_i}) / 3(\sigma_{xy_i} - X_{xy_i})$$

or :

$$dt\, k J_2(X_i)^{n-1} \left[X_{xy_i}(\sigma_{xx_i} - X_{xx_i}) / (\sigma_{xy_i} - X_{xy_i}) - X_{xx_i}\right] = dX_{xx_i} - dX_{xy_i}(\sigma_{xx_i} - X_{xx_i}) / (\sigma_{xy_i} - X_{xy_i})$$

A.3 - Equations expressing the consistency conditions in these layers

$$J_2(\sigma_i - X_i) = R_i$$

or by differentiating :

$$0 = 2(\sigma_{xx_i} - X_{xx_i})(d\sigma_{xx_i} - dX_{xx_i}) + 6(\sigma_{xy_i} - X_{xy_i})(d\sigma_{xy_i} - dX_{xy_i})$$

B - EQUATIONS PERTAINING TO THE LAYERS WHERE THERE IS PURE ELASTIC DEFORMATION

$$\text{if } J_2(\sigma_i - X_{io}) < R_i$$

B.1 - Strain/stress equations in these layers

(6) $$d\varepsilon_{xy} = \frac{d\sigma_{xyi}}{2\mu}$$

(7) $$d\varepsilon_{xx} = \frac{d\sigma_{xxi}}{E}$$

B.2 - Equations expressing the recovery in these layers

$$dX_{xxi} = -k J_2(X_i)^{n-1} X_{xxi}\, dt$$
$$dX_{xyi} = -k J_2(X_i)^{n-1} X_{xyi}\, dt$$

(evolution laws in the absence of plastic deformation).

C - The equations of the A and B paragraphs are linear in $d\varepsilon_{xx}$, $d\sigma_{xxi}$, $d\sigma_{xyi}$, dX_{xxi}, dX_{xyi} and can be resolved to express each of these unknowns as functions of $d\varepsilon_{xy}$.

This resolution allows to integrate ε_{xx}, σ_{xxi}, σ_{xyi}, X_{xxi} and X_{xyi} as functions of ε_{xy} and to calculate all these variables as the tensile/torsion numerical experiment proceeds.

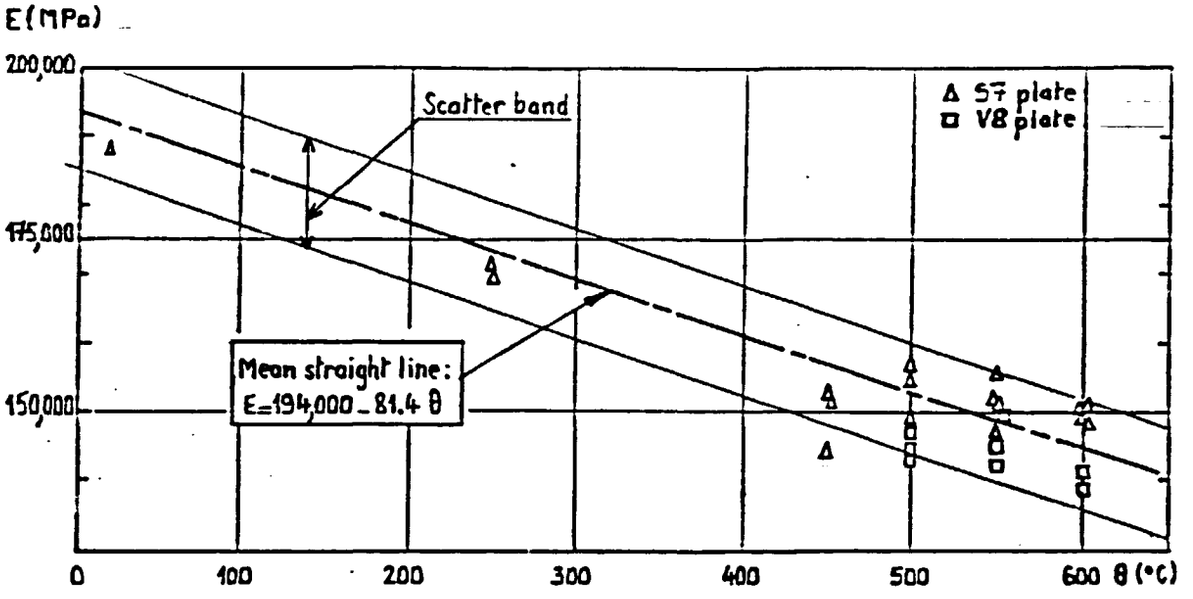

FIG. 2.1 17-12 Mo SPH steel. Variation of YOUNG's modulus E in terms of temperature θ.

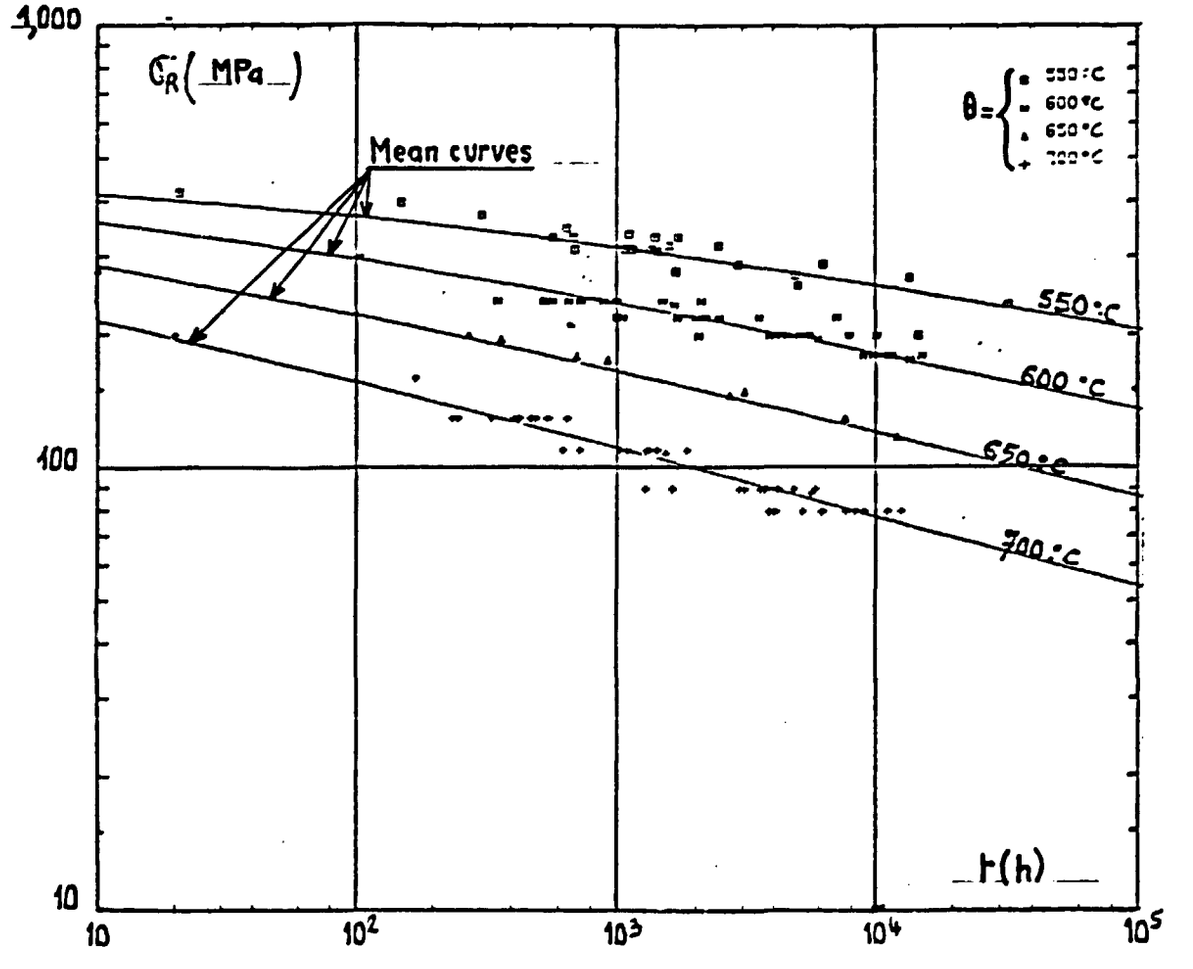

FIG. 2.3 17-12 Mo SPH steel. Creep rupture stress. Mean isothermal curves.

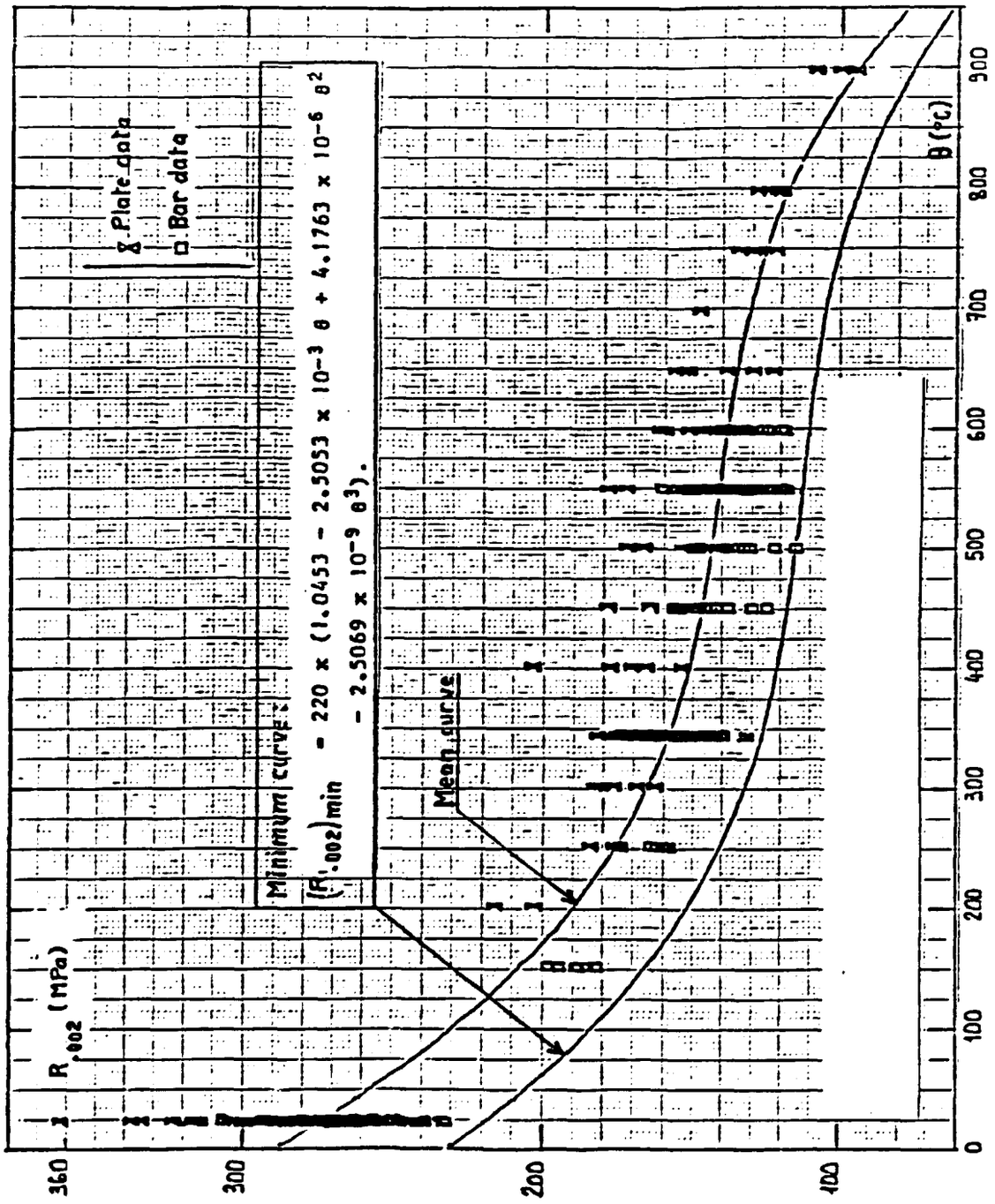

FIG. 2.2 17-12 Mo SPH steel. Variation of the .2% yield stress in terms of temperature.

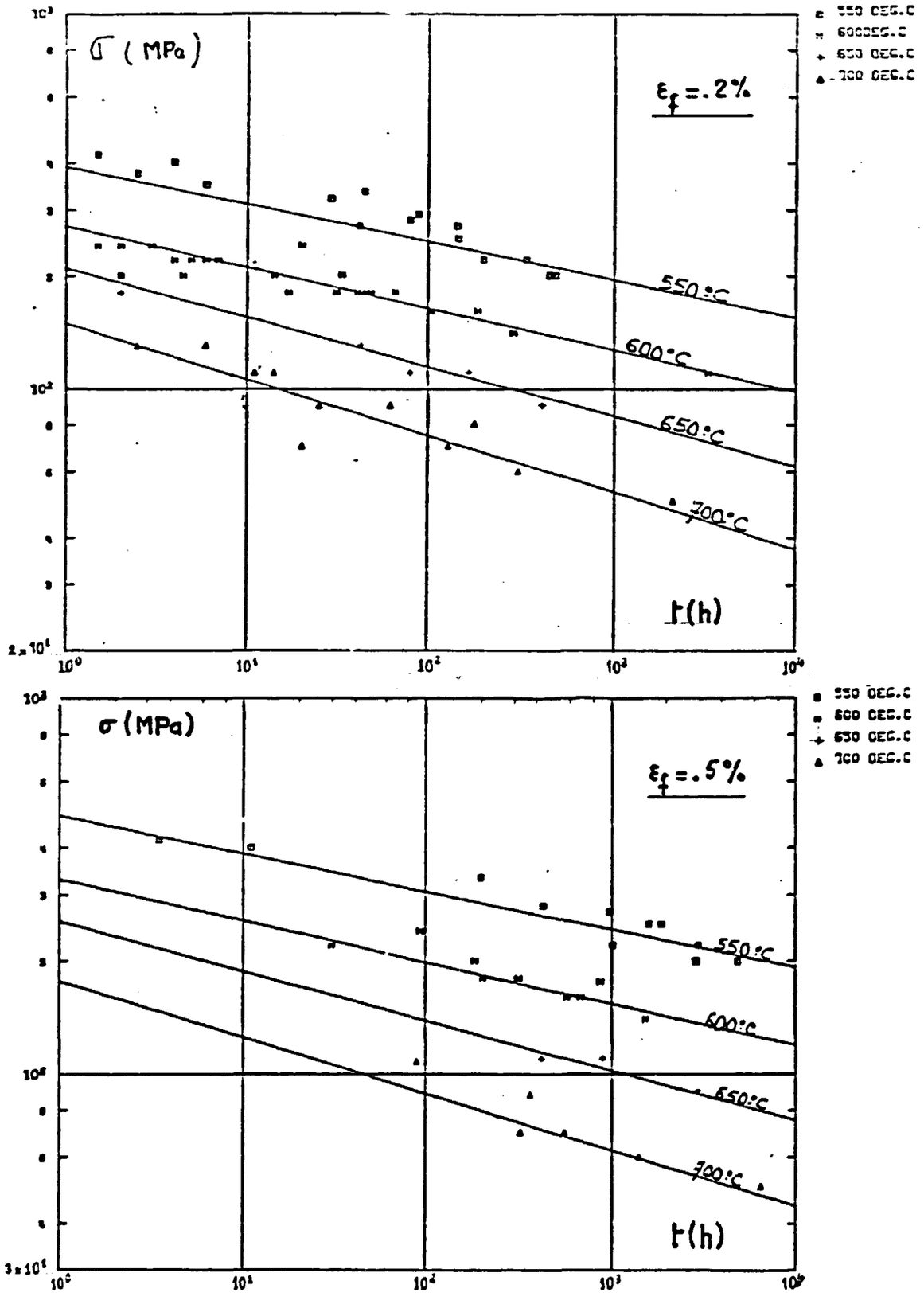

FIG. 2.4 17-12 Mo SPH steel. .2% and .5% creep strains. Mean isothermal curves.

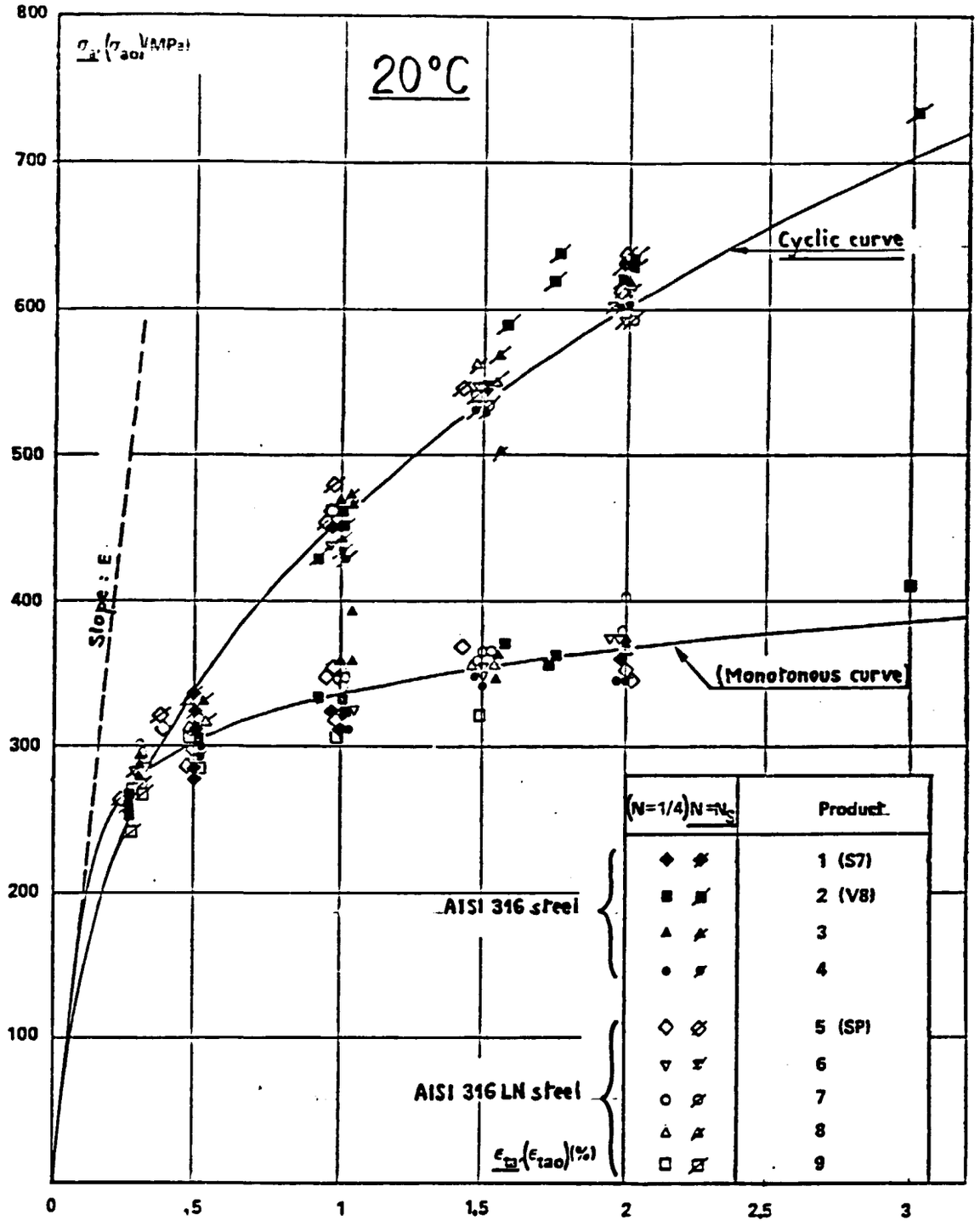

FIG. 2.5 a 17-12 Mo SPH steel. Hardening curves at 20°C.

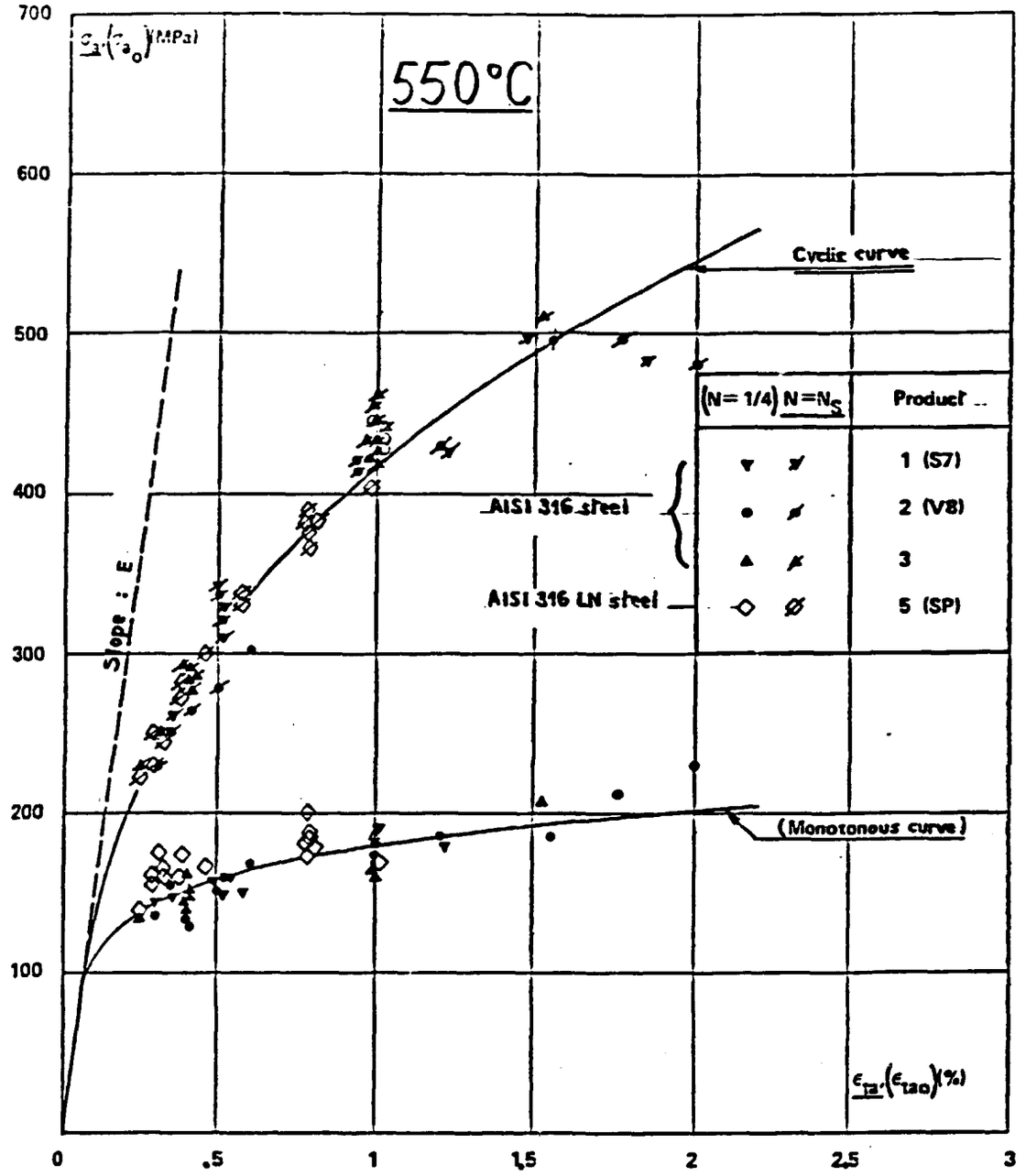

FIG. 2.5 b 17-12 Mo SPH steel. Hardening curves at 550°C.

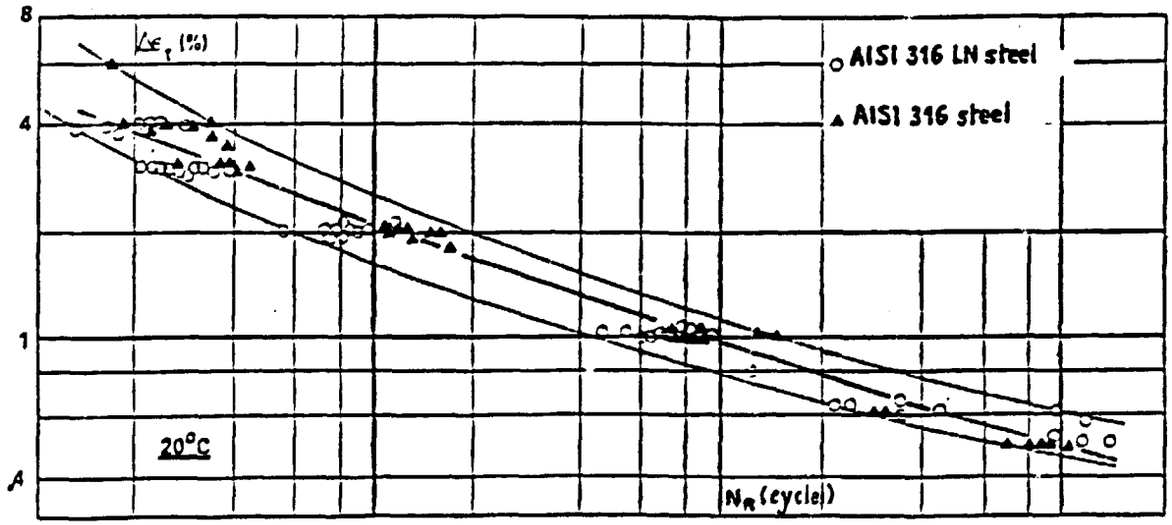

FIG. 2.6 17-12 Mo SPH steel. Low cycle fatigue strength curves at 20°C.

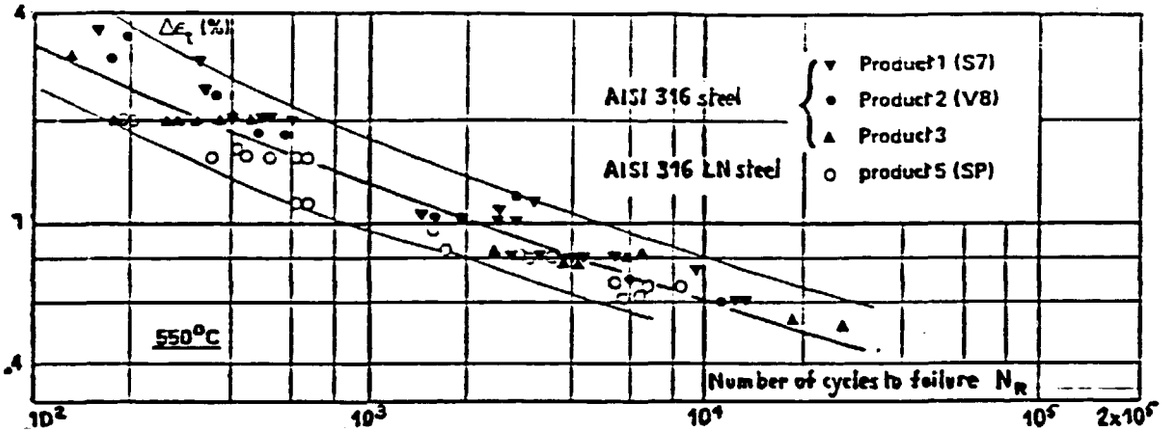

FIG. 2.6 (continued) 17-12 Mo SPH steel. Low cycle fatigue strength curves at 550°C.

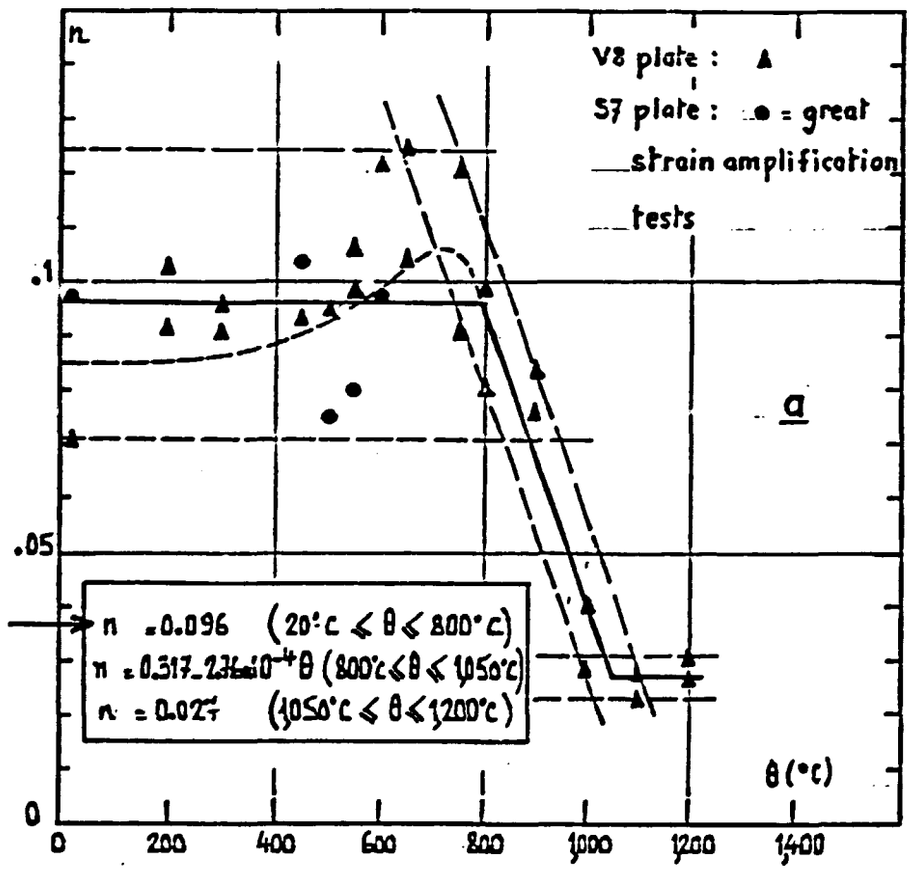

FIG. 2.7 a 17-12 Mo SPH steel. Tensile hardening equation ($\varepsilon_p \leq 1\%$). Variation of n in terms of temperature.

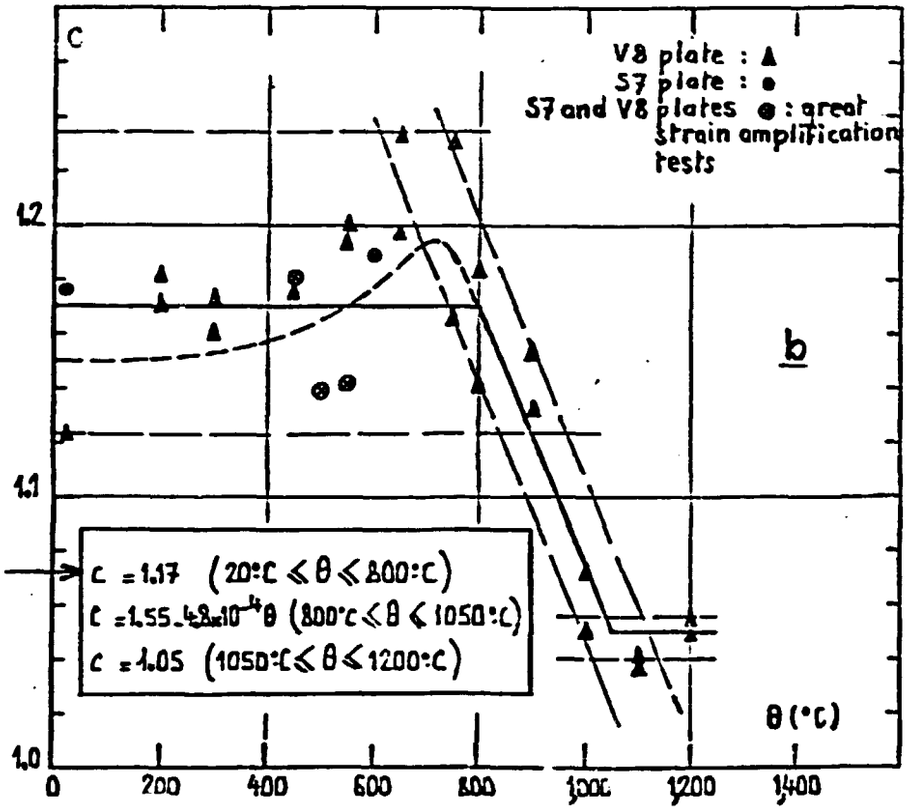

FIG. 2.7 b 17-12 Mo SPH steel. Tensile hardening equation ($\varepsilon_p \leq 1\%$). Variation of C in terms of temperature.

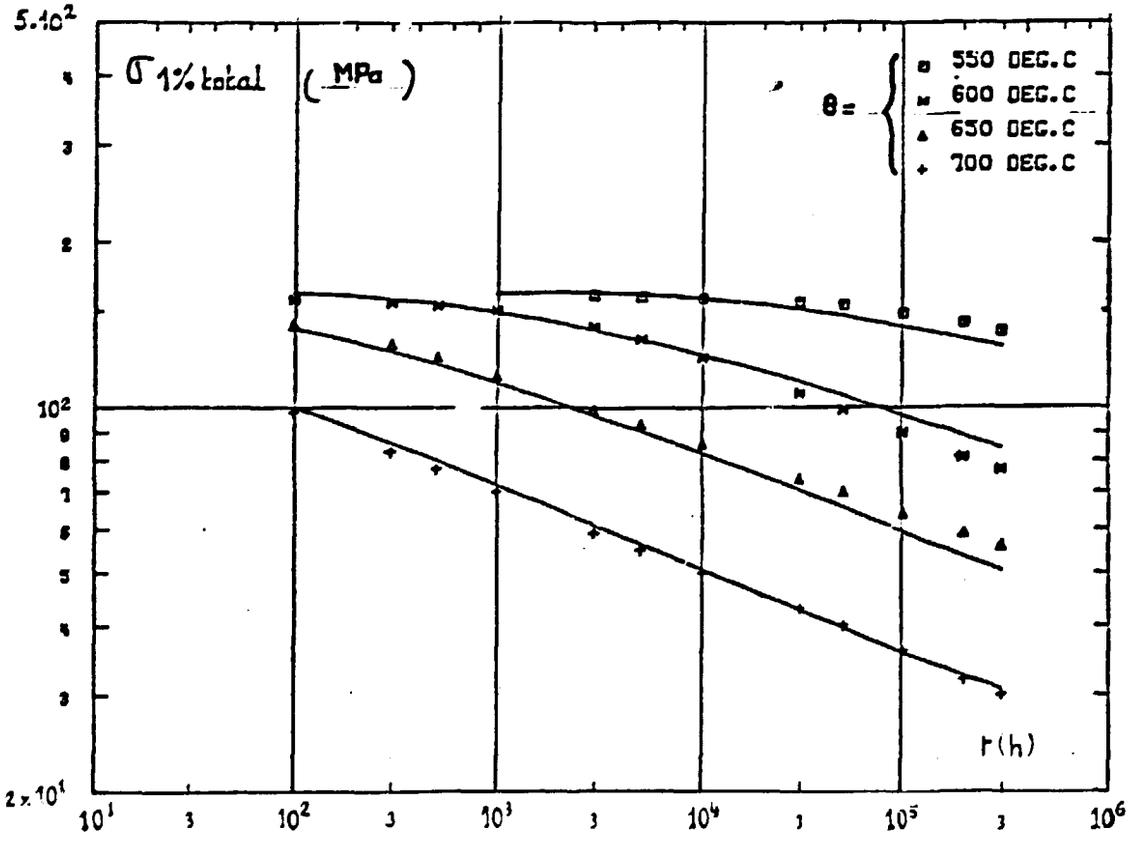

FIG. 2.8 17-12 Mo SPH steel. $\sigma_{1\%\ total}$ stress. Mean isothermal curves.

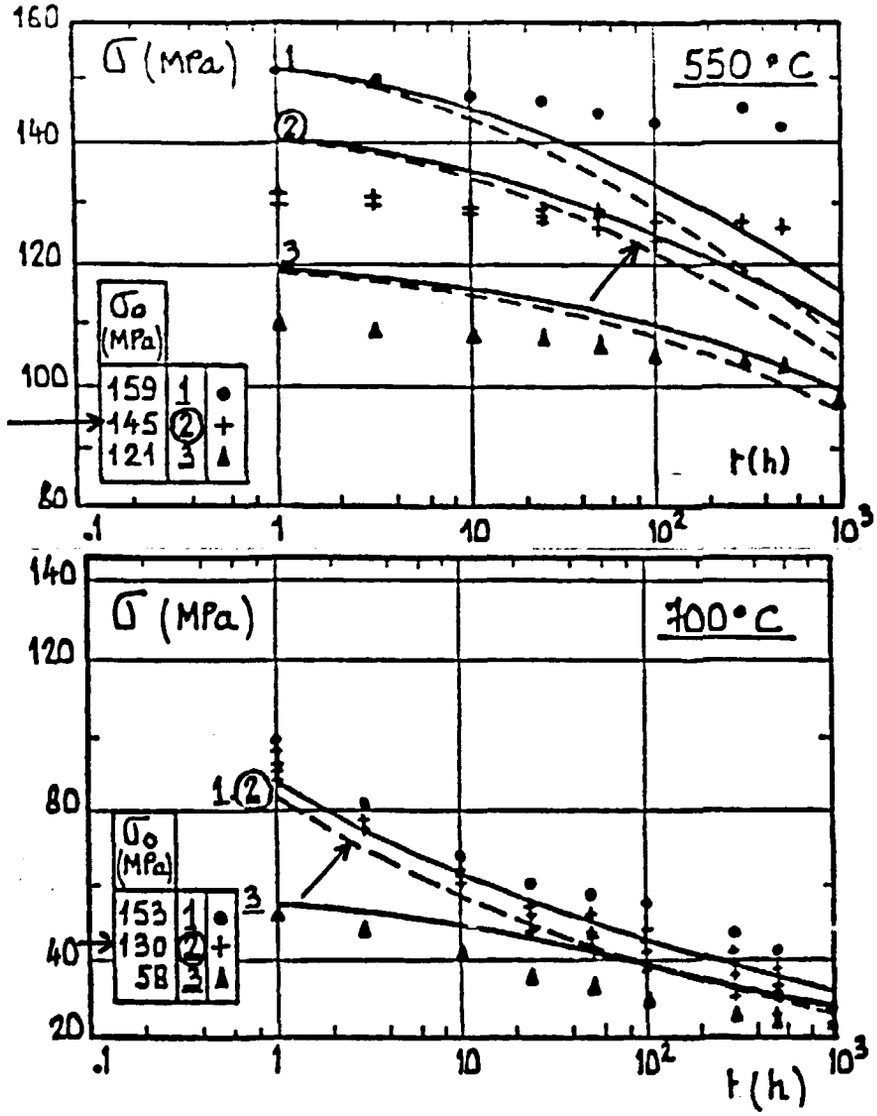

FIG. 2.9 17-12 Mo SPH steel. Stress relaxation comparison between the experimental points and the curves calculated with time hardening (- - -) or strain hardening (———) assumptions.

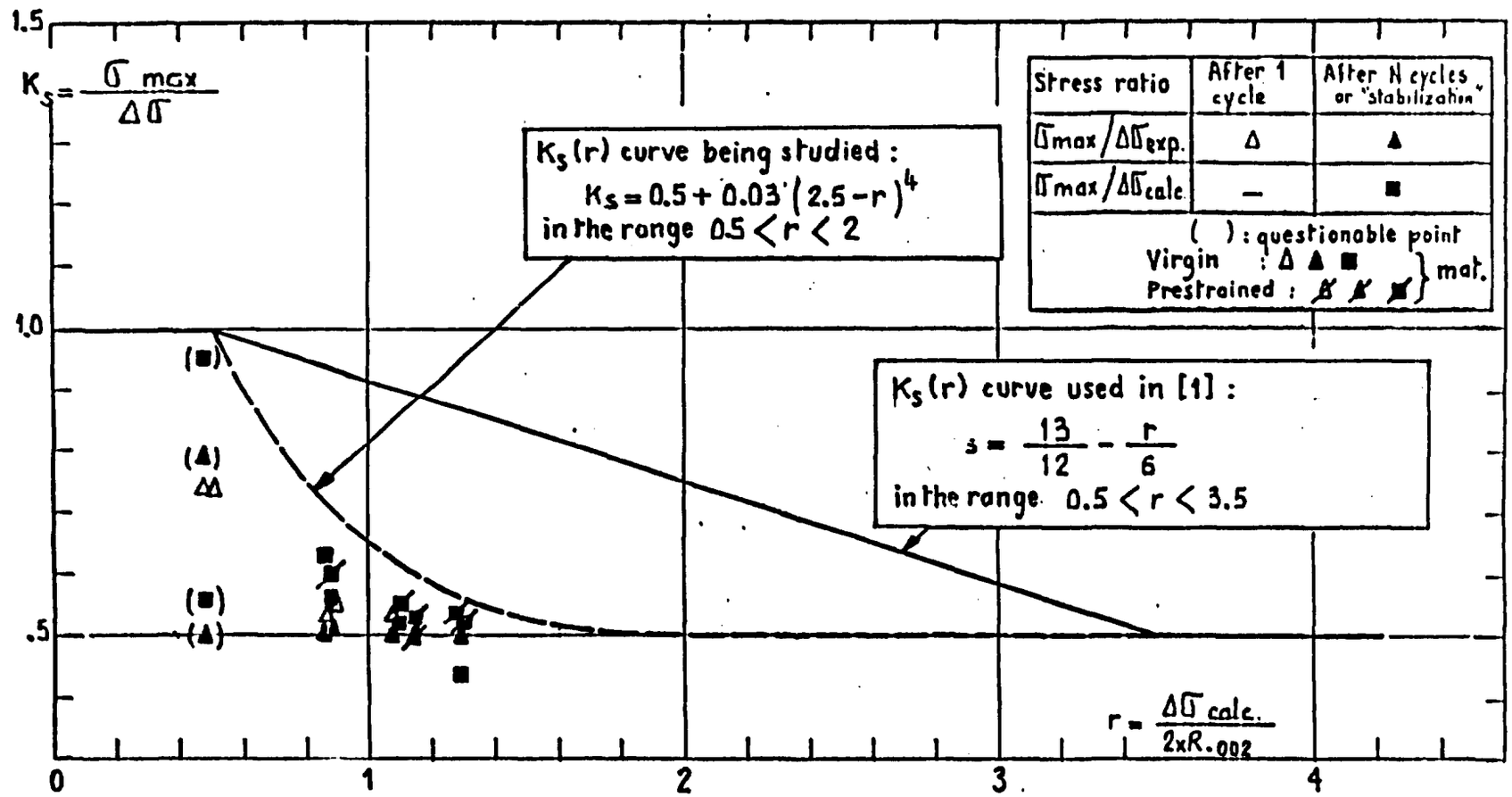

FIG. 2.10 17-12 Mo SPH steel. Plate at 550°C and 600°C. Variation of the "symetrisation" factor calculated with experimental data from $0\text{-}\varepsilon_T$ cycling in terms of $r = \Delta\sigma_{calc}/2xR_{.002}$.

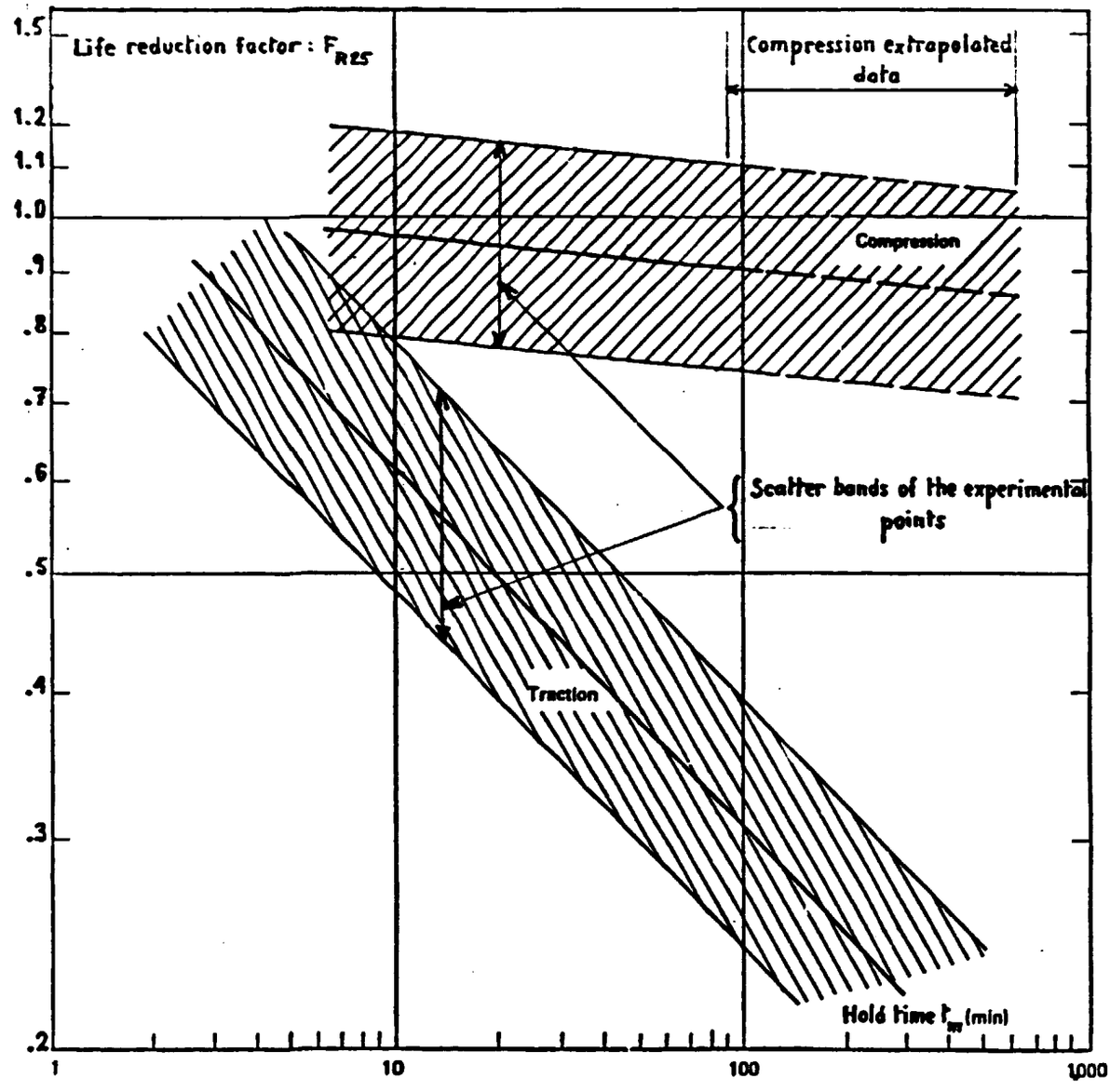

FIG. 2.11 17-12 Mo SPH steel. Plate at 600°C. Variation of the life reduction factor F_{R25} in terms of the duration and nature of the strain hold.

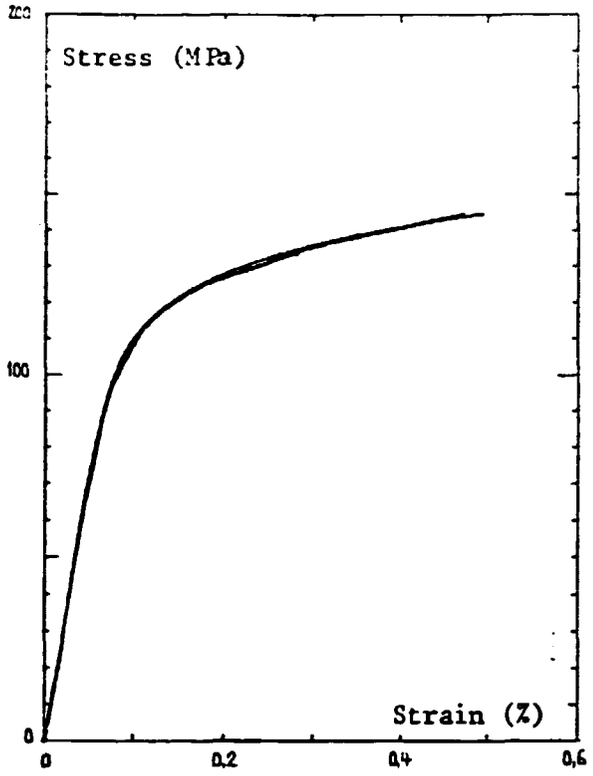

FIG. 3.1 Lower curve : ten layers model 650°C
Upper curve : tensile curve 650°C

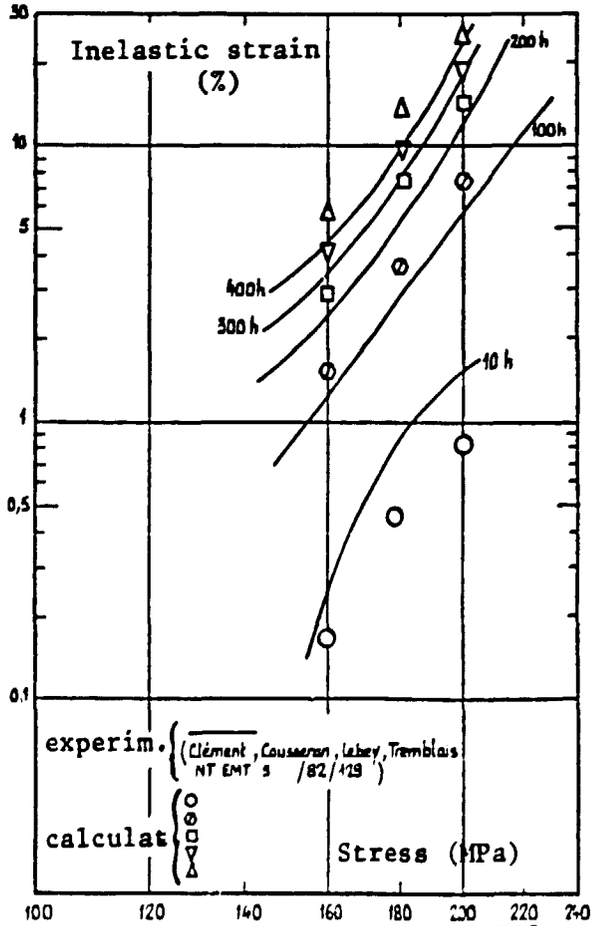

FIG. 3.2 Isochronous creep curves 650°C

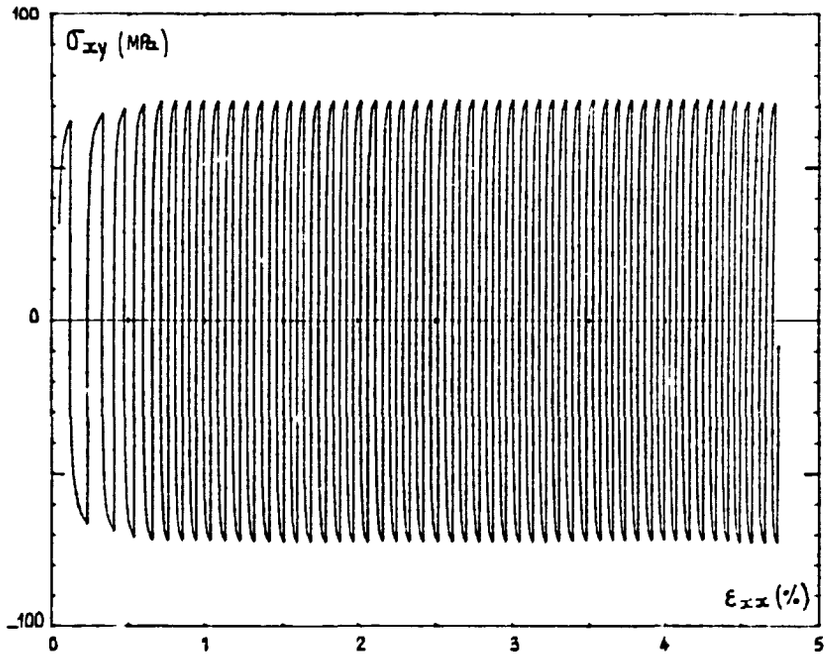

FIG. 3.3 $\left(\sigma_{xx}=70.1\ \text{MPa}\ ;\ \Delta\varepsilon_{xy}=3.10^{-3}\right)$ all the a_i coefficients = 100 MPa

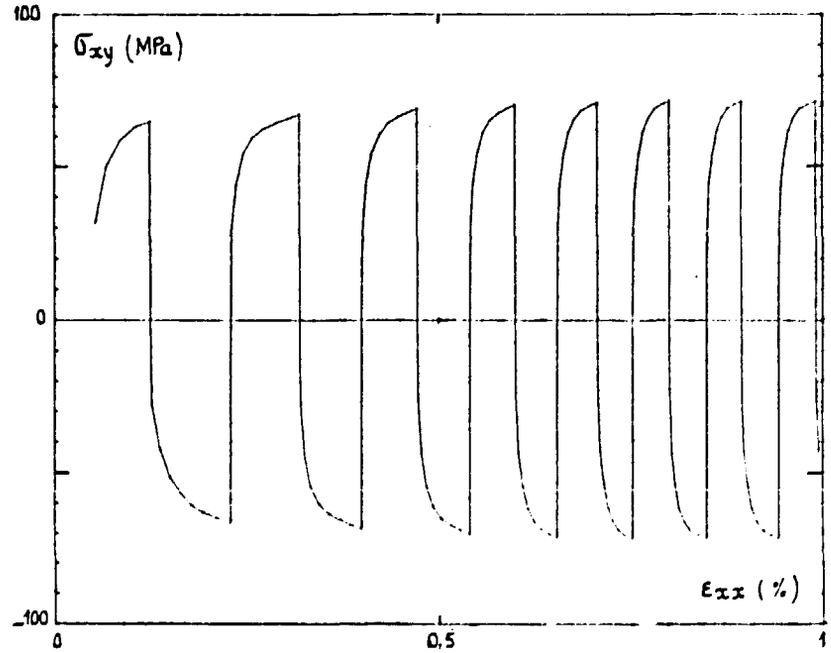

FIG. 3.3bis enlargement of FIG. 3.3

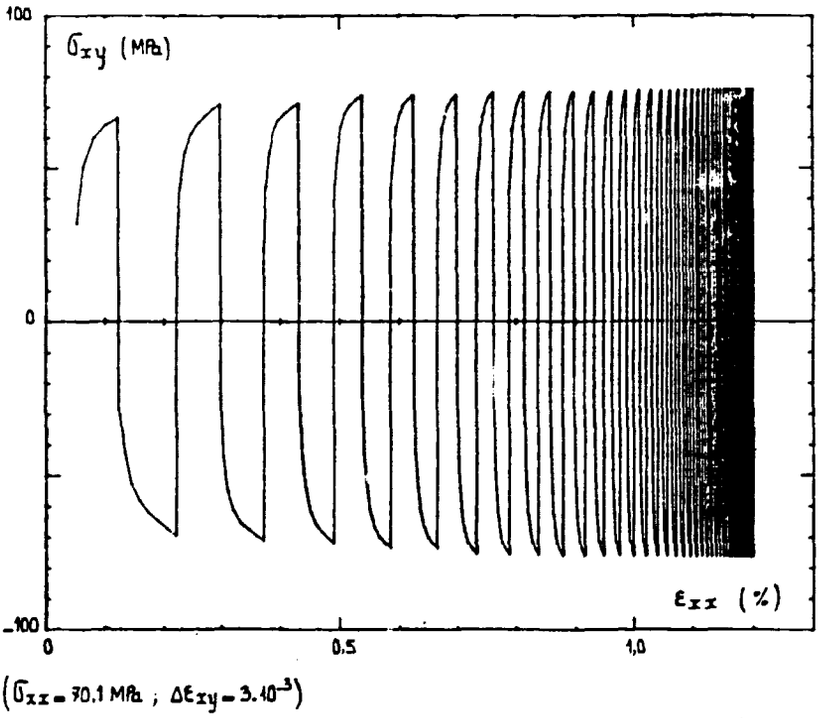

FIG. 3.4 The a_i coefficients are distributed in the 10^2 to 5.10^4MPa interval

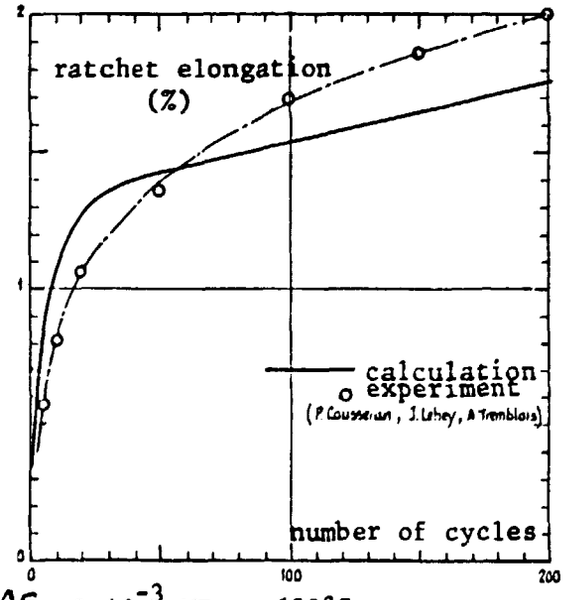

FIG. 3.5 σ_{xx}=78.7 MPa ; $\Delta\varepsilon_{xy}$=3.10^{-3} MPa ; 650°C

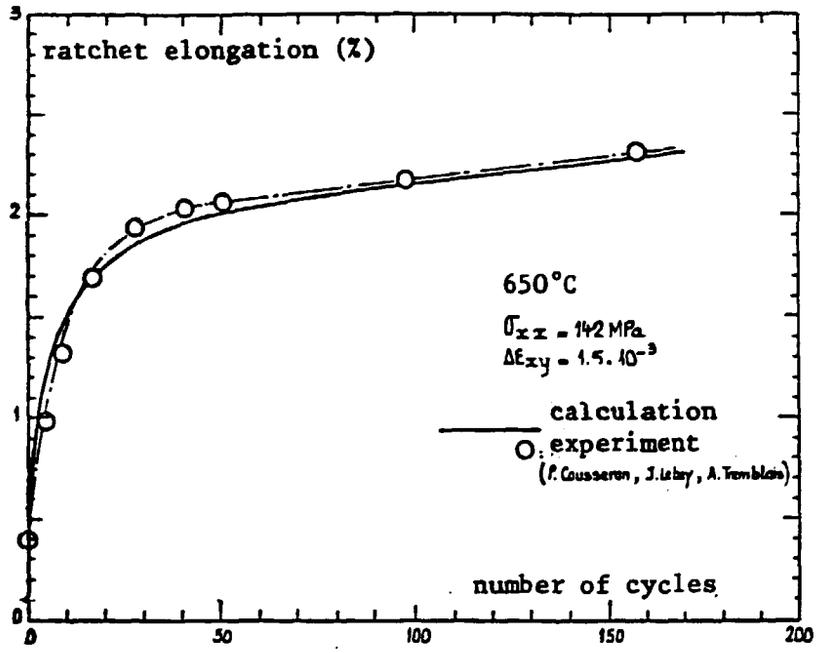
ratchet elongation (%)
650°C
σ_{xx} = 142 MPa
$\Delta\varepsilon_{xy}$ = 1.5. 10^{-3}
calculation
experiment
(P. Cousseran, J. Lebey, A. Tremblais)
number of cycles
0
1
2
3
0
50
100
150
200

FIG. 3.6

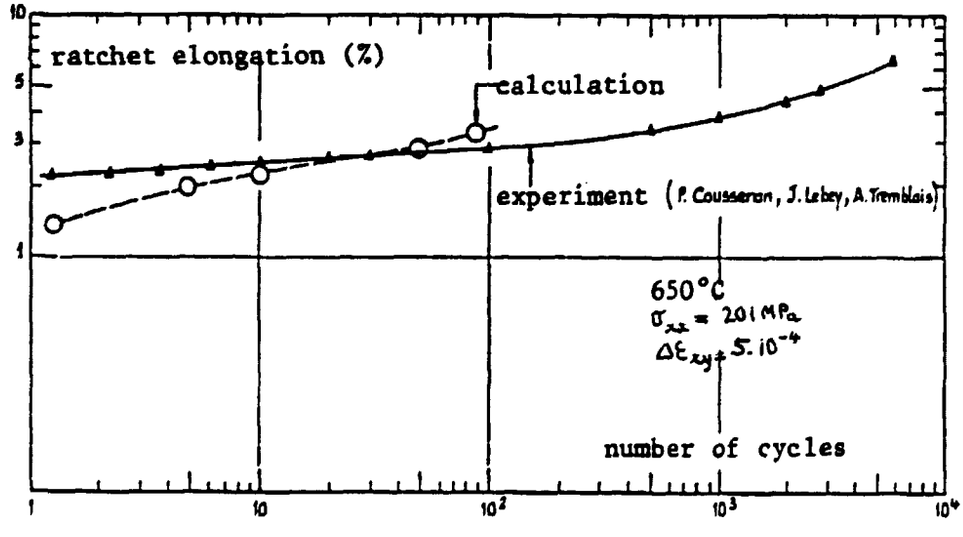
ratchet elongation (%)
calculation
experiment (P. Cousseran, J. Lebey, A. Tremblais)
650°C
σ_{xx} = 201 MPa
$\Delta\varepsilon_{xy}$ = 5. 10^{-4}
number of cycles
1
3
5
10
1
10
10^2
10^3
10^4

FIG. 3.7

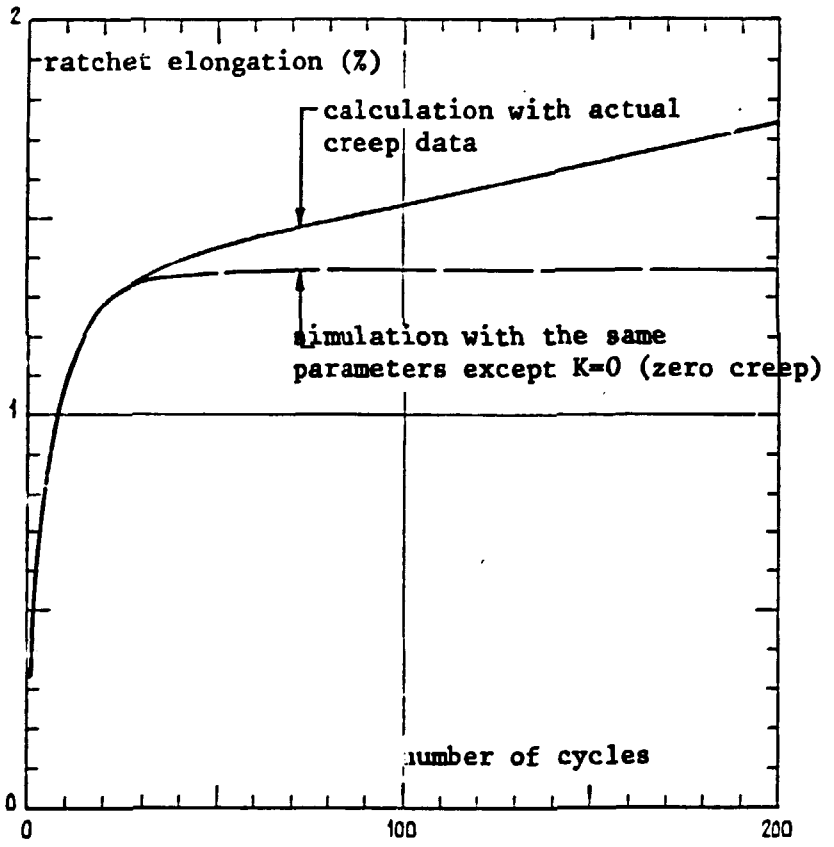

FIG. 3.8 650°C ; $\sigma_{xx} = 78.7$ MPa , $\Delta\varepsilon_{xy} = 3.10^{-3}$.

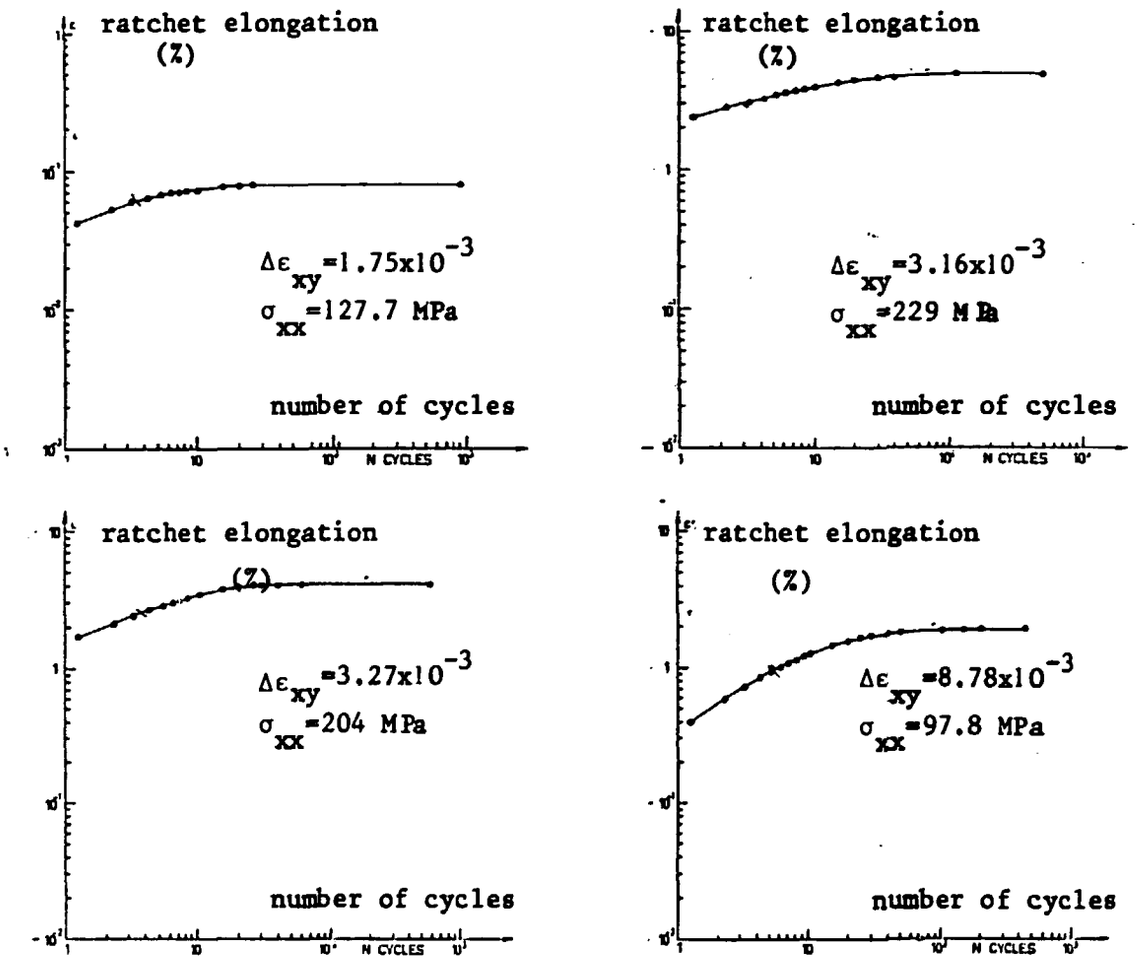

FIG. 3.9 Experiments Pierre COUTELLIER, Jacques LEBEY, Pierre CORBEL

300°C

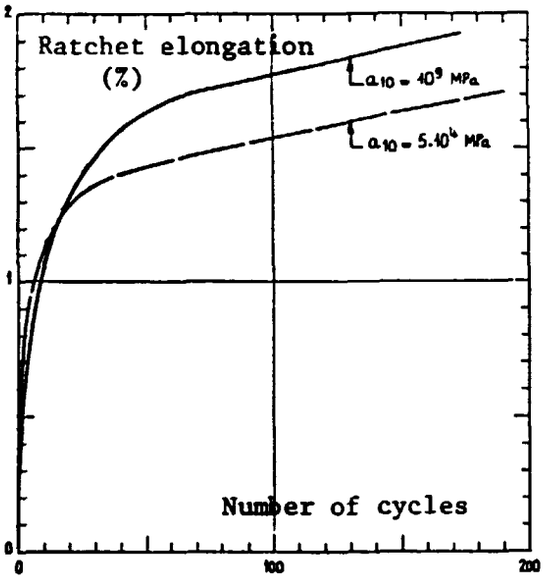

FIG. 3.10 σ_{xx}=78.7 MPa ; $\Delta\varepsilon_{xy}=3.10^{-3}$
Calculation with two a_i distributions :
the sole difference between these distributions being the a_{10} value.

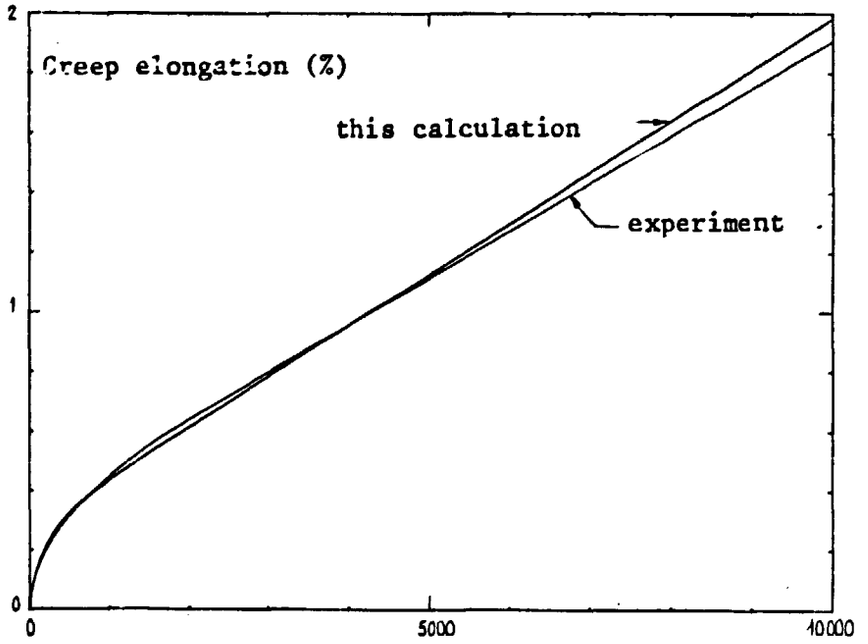

FIG. 3.11 Uniaxial creep curve
temperature : 600°C ; stress : 150 MPa
$a_{10} = 10^{12}$MPa

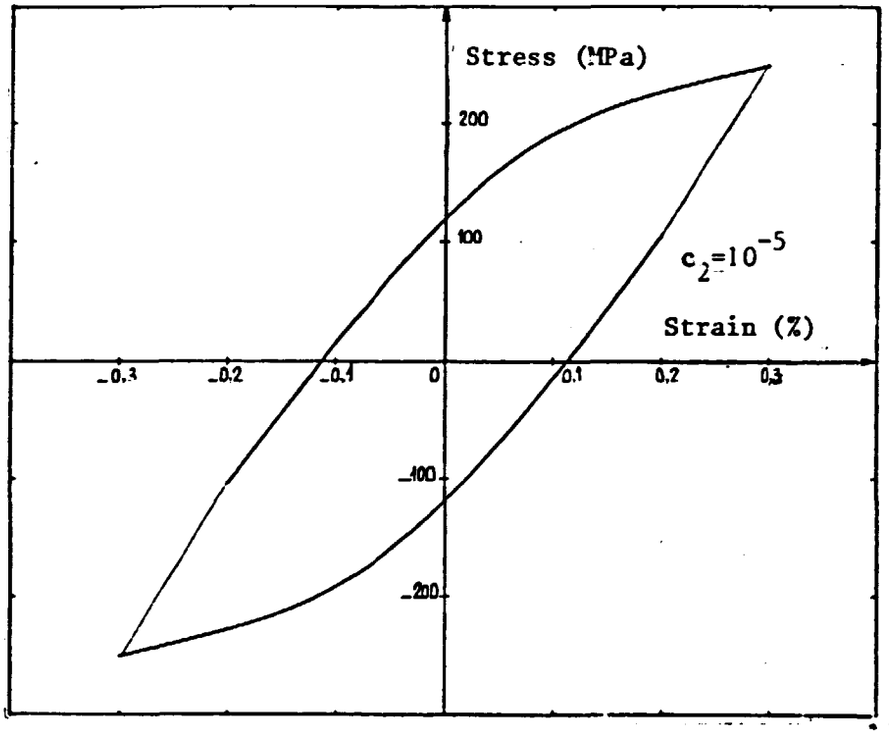

FIG. 3.12

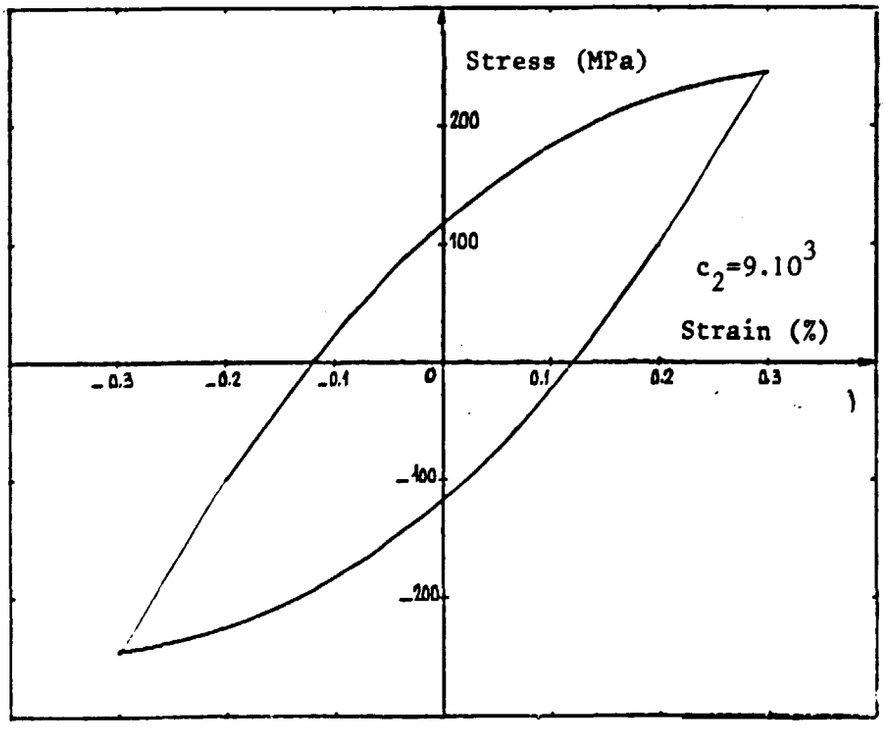

FIG. 3.13

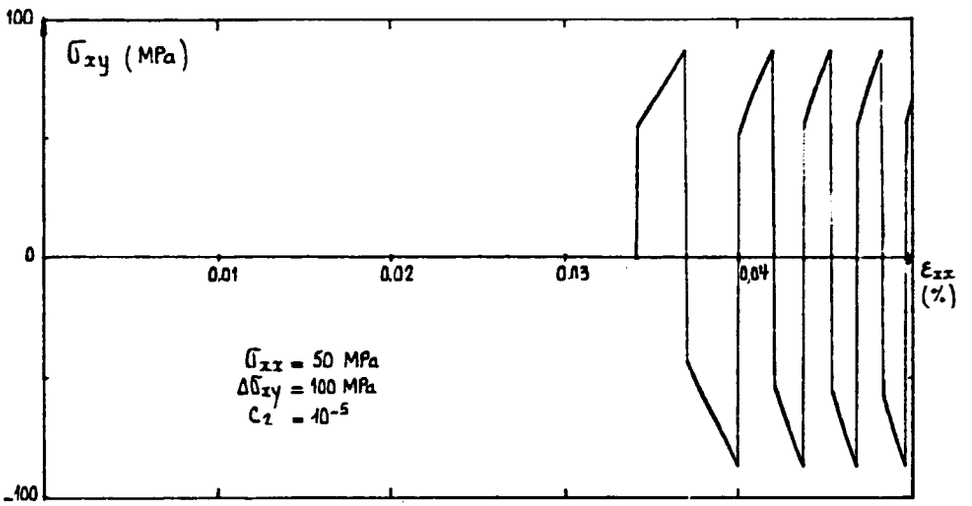

FIG. 3.14

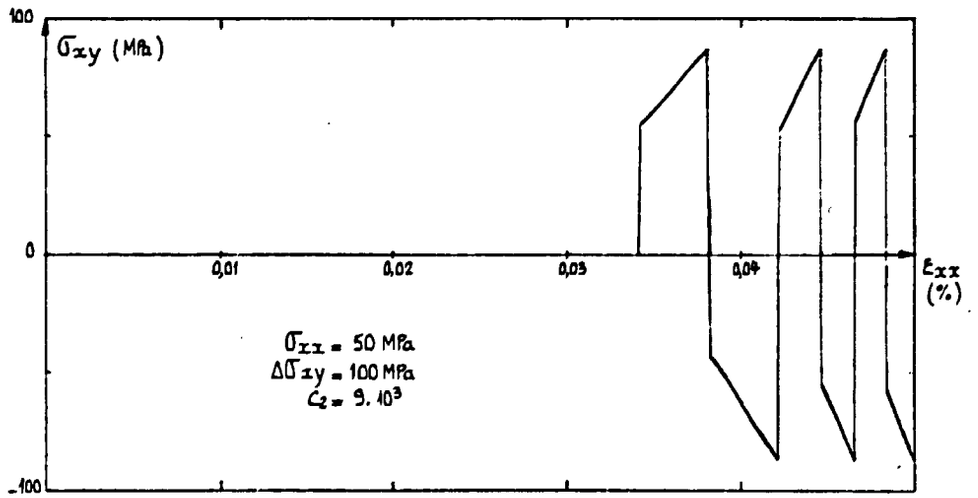

FIG. 3.15

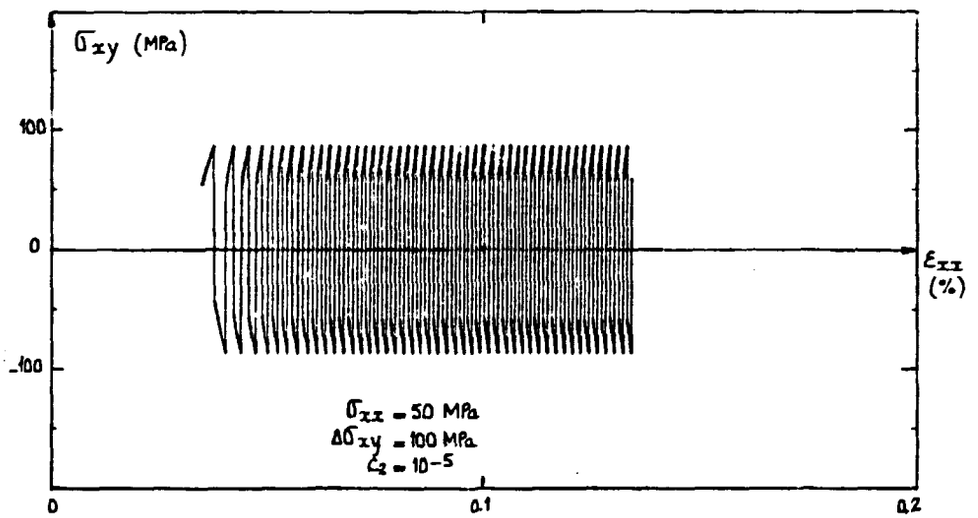

FIG. 3.16

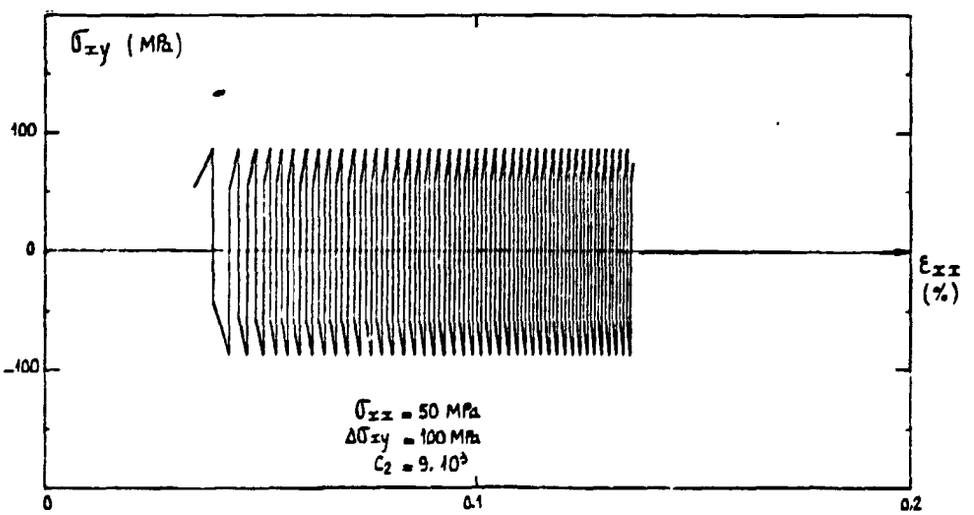

FIG. 3.17

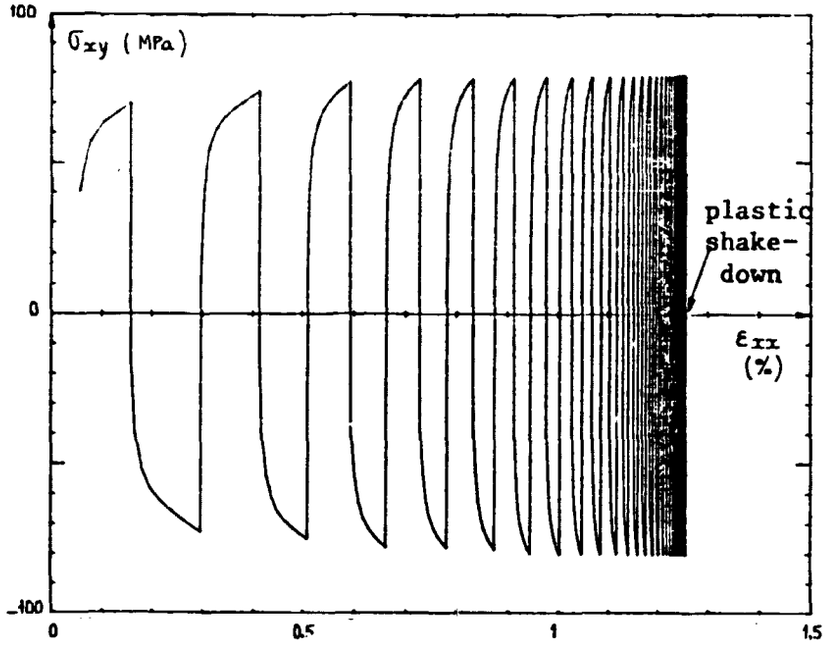

FIG. 3.18a σ_{xx}=100 MPa ; $\Delta\varepsilon_{xy}$=4.10^{-3}

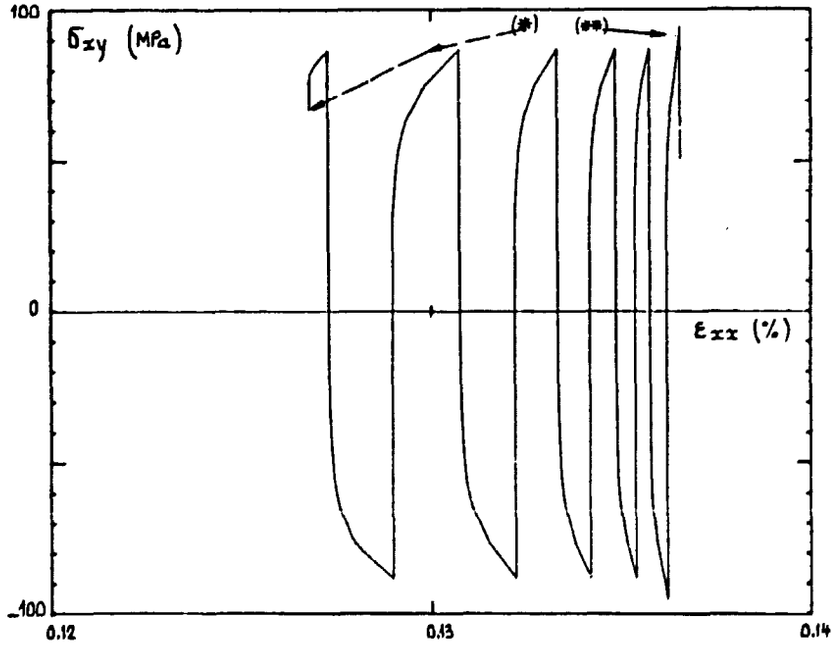

FIG. 3.18b This numerical experiment follows FIG. 3.18a with the same σ_{xx} and $\Delta\varepsilon_{xy}$=4.10^{-3} (*)
then with $\Delta\varepsilon_{xy}$ =8.10^{-3} (**)